Electronic Supplementary Material (ESI) for Dalton Transactions.

Supporting Information

Index:

1. Crystallographic data and selected bond lengths and angles.

Table S1. Crystallographic data for compounds **1**-**8**, **10** and **11**.

Complex	**1**	**2**	**3**	**4**	**5**
Formula	$C_{31}H_{43}Br_2DyN_4O_{17}Zn$	$C_{31}H_{43}Br_2ErN_4O_{17}Zn$	$C_{37}H_{32}Br_2DyN_5O_{12}Zn$	$C_{37}H_{32}Br_2ErN_5O_{12}Zn$	$C_{34}H_{32}Br_2Cl_2DyN_5O_{13}Zn$
M_r	1131.38	1136.14	1126.36	1131.12	1177.23
Crystal system	*monoclinic*	*monoclinic*	*triclinic*	*triclinic*	*monoclinic*
Space group (no.)	*I*2/*a*(15)	*I2/a(15)*	*P*-1(2)	*P*-1(2)	$P2_1/c$(14)
a (Å)	20.3151(2)	20.2750(4)	12.5528(6)	12.5279(5)	15.3456(13)
b (Å)	13.9186(1)	13.9256(3)	16.2599(8)	16.2474(5)	14.4928(10)
c (Å)	29.0441(5)	29.0584(12)	20.5009(7)	20.5317(8)	20.6419(15)
α (°)	90	90	105.887(4)	105.959(3)	90
β (°)	106.038(1)	106.096(3)	97.495(3)	97.486(3)	113.963(5)
γ (°)	90	90	104.095(4)	103.965(3)	90
V (Å^3)	7892.80(17)	7882.8(4)	3815.3(3)	3811.7(3)	4195.1(6)
Z	8	8	4	4	4
D_c (g cm^{-3})	1.904	1.915	1.961	1.971	1.864
μ(Mo/CuK_α) (mm^{-1})[a]	4.589	4.828	4.738	4.984	4.438
T (K)	100	100	100	100	100
Observed reflections	7333 (6563)	7313 (6442)	24556 (17128)	26524 (19434)	5305 (3970)
R_{int}	0.0234	0.0261	0.0362	0.0341	0.0691
Parameters	445	446	1052	1052	516
GOF	1.058	1.033	0.966	0.930	1.025
R_1[b,c]	0.0290 (0.0242)	0.0324 (0.0266)	0.0817(0.0472)	0.0512 (0.0306)	0.0666 (0.0389)
wR_2[d]	0.0541 (0.0521)	0.0657 (0.0632)	0.1233 (0.1106)	0.0595 (0.0570)	0.0803 (0.0710)
Largest difference in peak and hole (e Å^{-3})	2.129 and -1.071	2.480 and -1.277	2.784 and -1.983	1.237 and -1.164	0.720 and -0.652

[a]μ(CuK_α (mm^{-1}) in **1**. [b]$R_1 = S||F_o| - |F_c||/S|F_o|$. [c]Values in parentheses for reflections with $I > 2s(I)$. [d]$wR_2 = \{S[w(F_o^2 - F_c^2)^2] / S[w(F_o^2)^2]\}^{½}$

Table S1. Continuation.

Complex	**6**	**7**	**8**	**10**	**11**
Formula	$C_{34}H_{32}Br_2Cl_2ErN_5O_{13}Zn$	$C_{62}H_{80}Br_4Dy_2N_6O_{28}Zn_2$	$C_{62}H_{80}Br_4Er_2N_6O_{28}Zn_2$	$C_{31}H_{30}Br_2ErN_6O_{13}Zn$	$C_{31}H_{31}Br_2ErN_6O_{14}Zn$
M_r	1181.99	2132.70	2142.22	1082.30	1104.07
Crystal system	*monoclinic*	*triclinic*	*monoclinic*	*monoclinic*	*monoclinic*
Space group (no.)	$P2_1/n$ (14)	P-1(2)	$P2_1/c$(14)	$I2/a$ *(15)*	$P2_1/n$ (14)
a (Å)	15.2858(6)	11.960(5)	12.0449(5)	20.3420(6)	13.516(5)
b (Å)	14.4617(5)	13.985(5)	22.2693(10)	14.7835(4)	20.775(5)
c (Å)	20.0422(7)	24.559(5)	28.4885(14)	28.2615(12)	13.539(5)
α (°)	90	97.150(5)	90	90	90
β (°)	110.541(2)	95.160(5)	90.500(2)	106.543(4)	91.534(5)
γ (°)	90	110.313(5)	90	90	90
V (Å^3)	4148.8(3)	3783(5)	7641.2(6)	8147.2(5)	3800(2)
Z	4	2	4	8	4
D_c (g cm^{-3})	1.892	1.895	1.862	1.712	1.930
μ(MoK_α) (mm^{-1})	4.710	4.777	4.968	4.657	5.000
T (K)	100	100	100	100	100
Observed reflections	10765 (7523)	16108 (12080)	19612 (15322)	7552 (5364)	9864 (7886)
R_{int}	0.0756	0.0581	0.0602	0.0935	0.1243
Parameters	516	951	958	445	501
GOF	1.017	0.979	1.165	0.998	1.078
R_1[a,b]	0.0795 (0.0414)	0.0645 (0.0446)	0.0779 (0.0522)	0.0726 (0.0455)	0.0666 (0.0465)
wR_2[c]	0.0904 (0.0778)	0.0987 (0.0905)	0.1154 (0.1071)	0.1050 (0.0934)	0.1088 (0.1007)
Largest difference in peak and hole (e Å^{-3})	1.380 and -1.024	1.456 and -1.053	2.441 and -2.029	1.495 and -0.961	2.989 and -1.906

[a] $R_1 = S||F_o| - |F_c||/S|F_o|$. [b] Values in parentheses for reflections with $I > 2s(I)$. [c] $wR_2 = \{S[w(F_o^2 - F_c^2)^2] / S[w(F_o^2)^2]\}^{½}$

Table S2. Selected bond lengths (Å) and angles (°) for complexes **1-8**, **10** and **11**.

Complex	**1**	**2**	**3**	**4**	**5**	**6**	**7**	**8**	**10**	**11**
Ln(1)···Zn(1)	3.3764(4)	3.3692(4)	3.3740(10)	3.3523(6)	3.3715(9)	3.3527(5)	3.3287(13)	3.3195(8)	3.3622(7)	3.3623(7)
Ln(2)···Zn(2)			3.3688(10)	3.3597(6)			3.3858(9)	3.3201(8)		
Ln(1)···Ln(2)							3.7400(9)	3.6774(4)		
Ln(1)-O(1A)	2.351(2)	2.341(3)	2.339(5)	2.305(3)	2.360(5)	2.342(3)	2.393(4)	2.352(5)	2.320(4)	2.316(4)
Ln(1)-O(2A)	2.337(2)	2.364(2)	2.362(5)	2.378(3)	2.331(5)	2.306(3)	2.353(4)	2.313(4)	2.356(4)	2.364(4)
Ln(1)-O(3A)	2.380(2)	2.318(2)	2.370(5)	2.342(3)	2.380(5)	2.363(3)	2.340(4)	2.319(4)	2.308(4)	2.282(4)
Ln(1)-O(21A)							2.324(3)	2.315(4)		
Ln(1)-O(21B)							2.213(3)	2.208(4)		
Ln(1)-O(22A)							2.470(3)	2.425(4)		
Ln(1)-O(4A)	2.363(2)	2.334(3)	2.372(5)	2.340(3)	2.365(5)	2.335(3)			2.343(4)	2.338(4)
Ln(1)-O(1C)	2.291(3)	2.273(3)	2.327(5)	2.312(3)	2.289(5)	2.264(3)	2.346(3)	2.305(4)	2.308(4)	2.342(4)
Ln(1)-O(1E)	2.454(3)	2.459(3)	2.433(5)	2.405(3)	2.438(5)	2.415(3)		2.333(5)	2.431(5)	2.375(4)
Ln(1)-O(2E)	2.472(2)	2.435(2)	2.423(5)	2.427(3)	2.458(5)	2.447(3)			2.435(4)	2.461(4)
Ln(1)-O(1F)	2.464(3)	2.440(3)	2.464(5)	2.411(3)	2.496(5)	2.447(3)	2.371(4)		2.428(4)	2.413(4)
Ln(1)-O(2F)	2.481(2)	2.466(3)	2.495(5)	2.443(3)	2.484(5)	2.477(3)			2.466(4)	2.485(4)
Ln(2)-O(1B)			2.320(5)	2.322(3)			2.403(4)	2.368(4)		
Ln(2)-O(2B)			2.408(5)	2.341(3)			2.362(3)	2.325(4)		
Ln(2)-O(3B)			2.362(5)	2.352(3)			2.378(4)	2.313(4)		
Ln(2)-O(4B)			2.354(5)	2.347(3)						
Ln(2)-O(21A)							2.255(3)	2.197(4)		
Ln(2)-O(21B)							2.353(3)	2.303(4)		
Ln(2)-O(22B)							2.459(3)	2.502(4)		

Table S2. Continuation.

Complex	**1**	**2**	**3**	**4**	**5**	**6**	**7**	**8**	**10**	**11**
Ln(2)-O(1D)			2.325(5)	2.303(3)			2.395(3)	2.314(4)		
Ln(2)-O(1E)							2.491(4)			
Ln(2)-O(1F)								2.339(5)		
Ln(2)-O(2E)							2.550(4)			
Ln(2)-O(1G)			2.431(6)	2.404(3)						
Ln(2)-O(2G)			2.449(6)	2.404(3)						
Ln(2)-O(1H)			2.444(6)	2.427(3)						
Ln(2)-O(2H)			2.467(6)	2.477(3)						
Zn(1)-N(1A)	2.109(2)	2.110(3)	2.096(6)	2.100(3)	2.107(6)	2.095(4)	2.105(5)	2.100(6)	2.120(5)	2.132(5)
Zn(1)-N(2A)	2.105(3)	2.105(3)	2.106(6)	2.128(3)	2.130(6)	2.126(4)	2.109(4)	2.110(6)	2.085(5)	2.110(5)
Zn(1)-O(2A)	2.125(2)	2.068(2)	2.070(5)	2.048(3)	2.131(5)	2.116(3)	2.101(3)	2.105(4)	2.053(4)	2.072(4)
Zn(1)-O(3A)	2.063(2)	2.124(3)	2.086(5)	2.078(3)	2.087(5)	2.076(3)	2.016(4)	2.019(4)	2.133(4)	2.087(4)
Zn(1)-O(2C)	1.958(2)	1.957(3)	1.997(5)	1.981(3)	1.977(5)	1.974(3)	1.985(4)	1.987(5)	1.973(4)	1.996(4)
Zn(2)-N(1B)			2.103(6)	2.100(3)			2.080(4)	2.088(6)		
Zn(2)-N(2B)			2.131(6)	2.107(3)			2.120(5)	2.121(6)		
Zn(2)-O(2B)			2.047(5)	2.072(3)			2.119(4)	2.108(4)		
Zn(2)-O(3B)			2.072(5)	2.082(3)			1.989(4)	2.011(4)		
Zn(2)-O(2D)			1.986(5)	1.989(3)			1.984(4)	1.984(5)		
Ln(1)-O(2A)-Zn(1)	98.26(8)	98.77(9)	98.92(19)	98.18(11)	98.05(19)	98.51(12)	96.58(13)	97.31(17)	99.16(15)	98.36(14)

Table S2. Continuation.

Complex	**1**	**2**	**3**	**4**	**5**	**6**	**7**	**8**	**10**	**11**
Ln(1)-O(3A)-Zn(1)	98.65(8)	98.46(9)	98.21(19)	98.49(10)	97.81(18)	97.90(12)	99.42(14)	99.61(17)	98.35(16)	100.55(15)
Ln(2)-O(2B)-Zn(2)			97.93(19)	98.96(10)			98.00(13)	96.90(16)		
Ln(2)-O(3B)-Zn(2)			98.65(19)	98.33(10)			101.24(14)	100.11(17)		
Ln(1)-O(21A)-Ln(2)							109.53(13)	109.16(17)		
Ln(1)-O(21B)-Ln(2)							109.96(13)	109.19(16)		

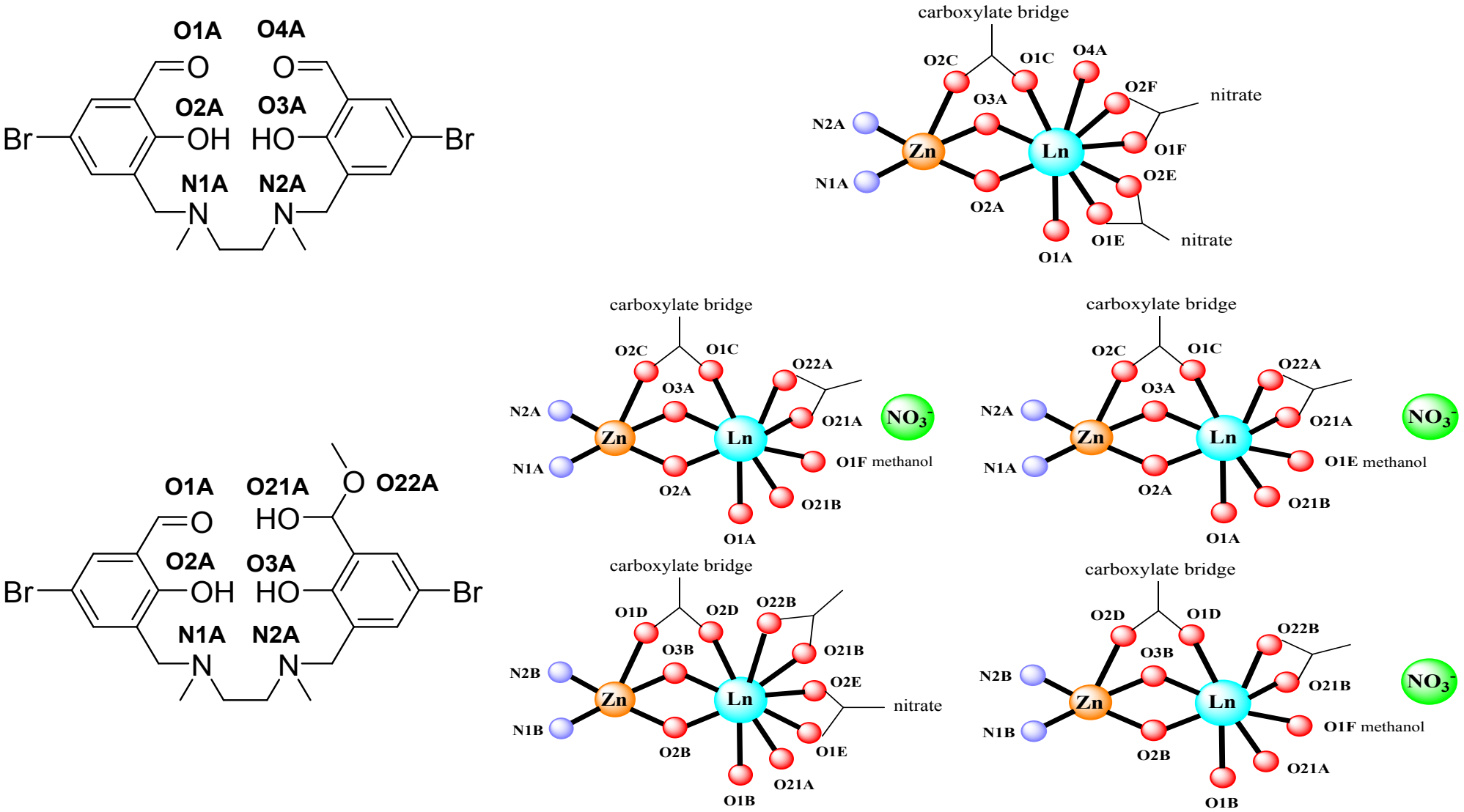

Figure S1. Ligand scheme (left) and labelling scheme (right) used in table S2 for complexes **1-6** and **10-11** (up)**, 7**(down left) and **8** (down right).

2. Experimental PXRD.

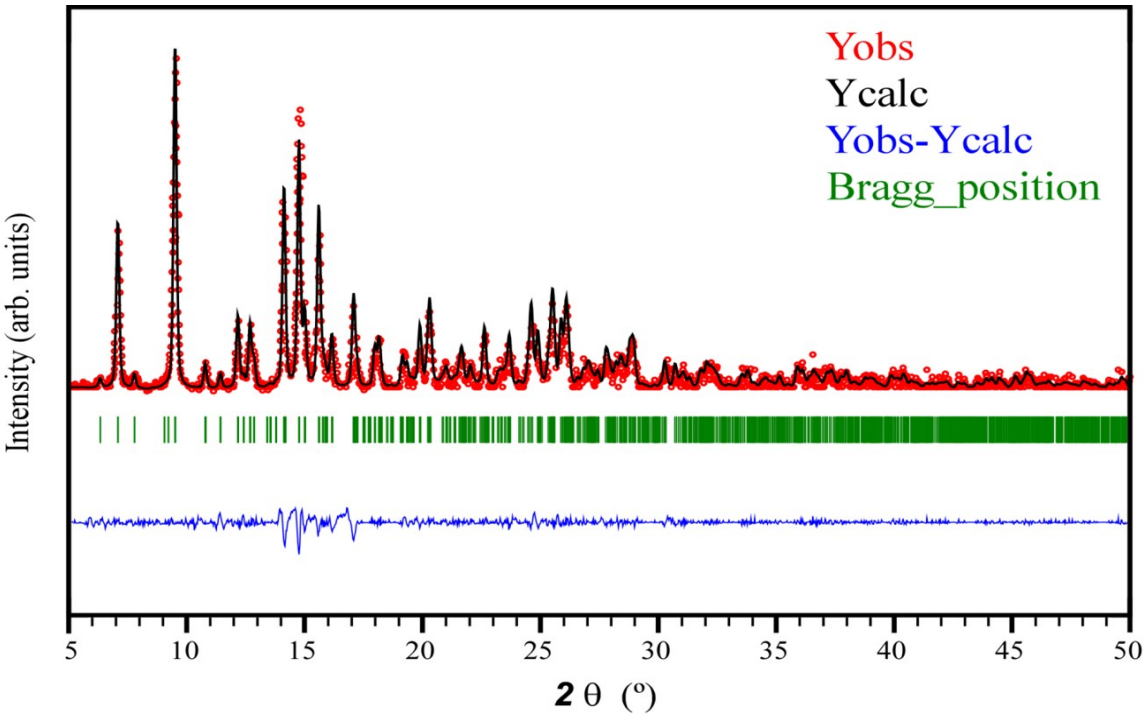

Compound 1

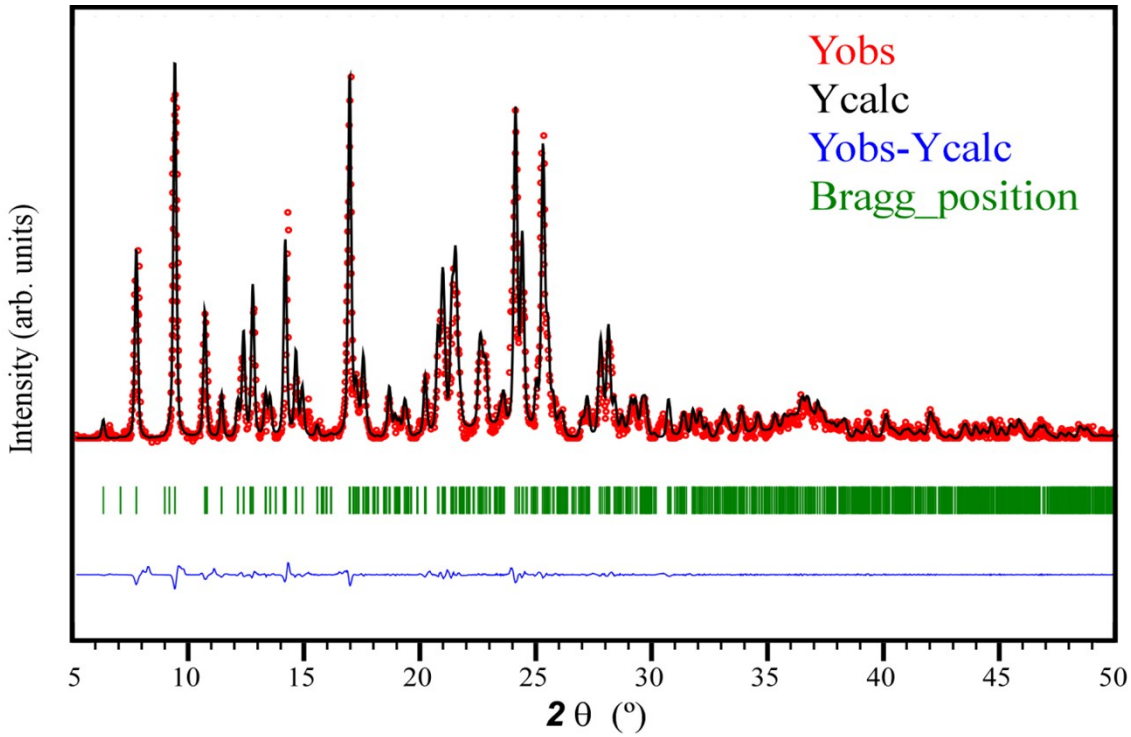

Compound 2

Figure S2. Pattern-matching analyses and experimental PXRD for complexes **1**-**2**.

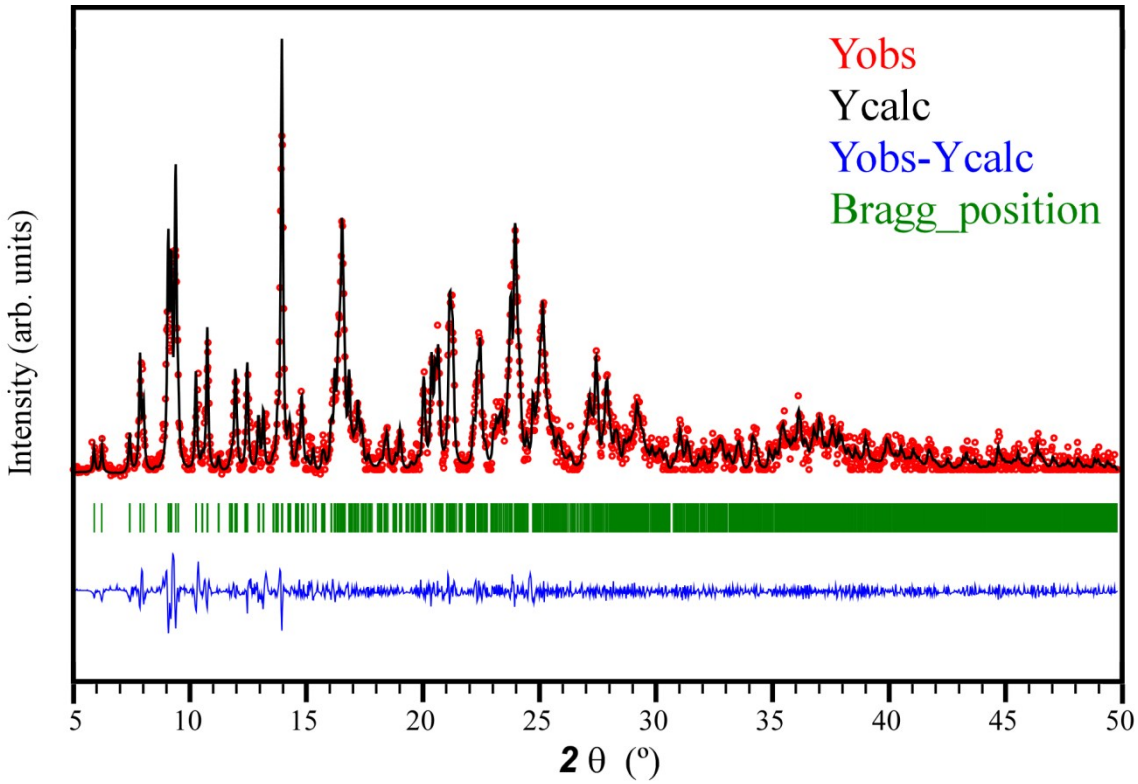

Compound 3

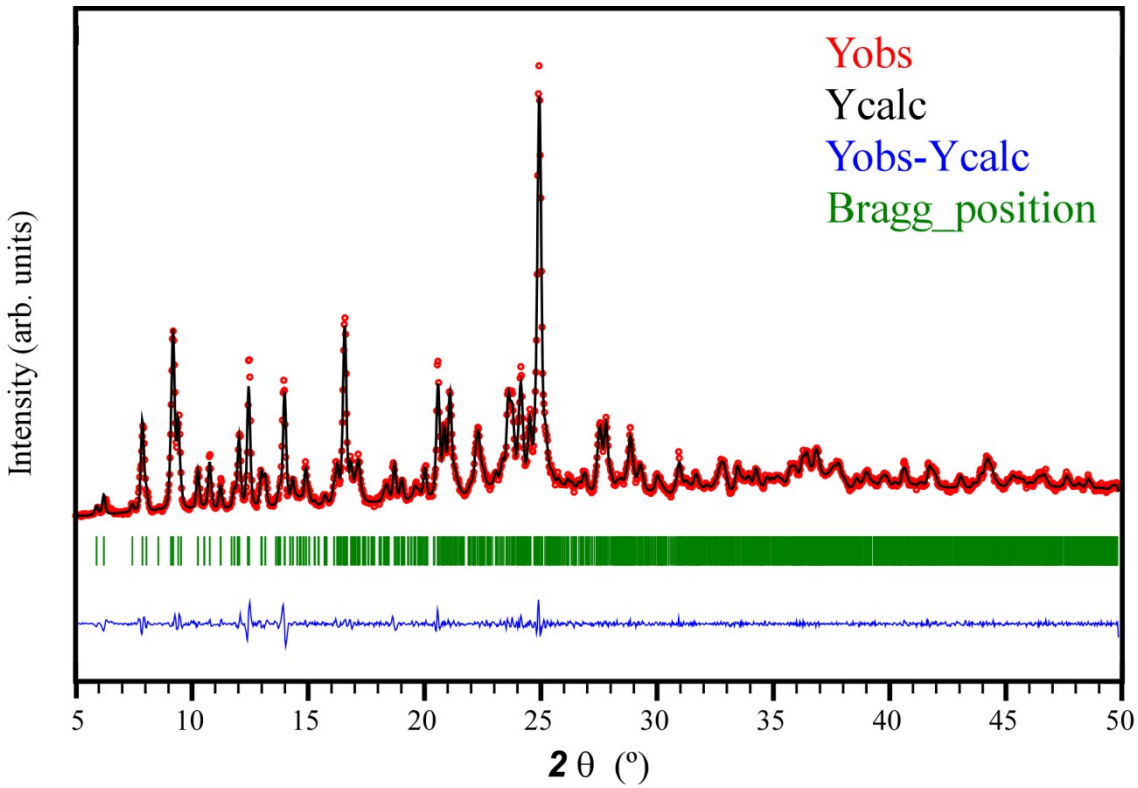

Compound 4

Figure S3. Pattern-matching analyses and experimental PXRD for complexes **3-4**.

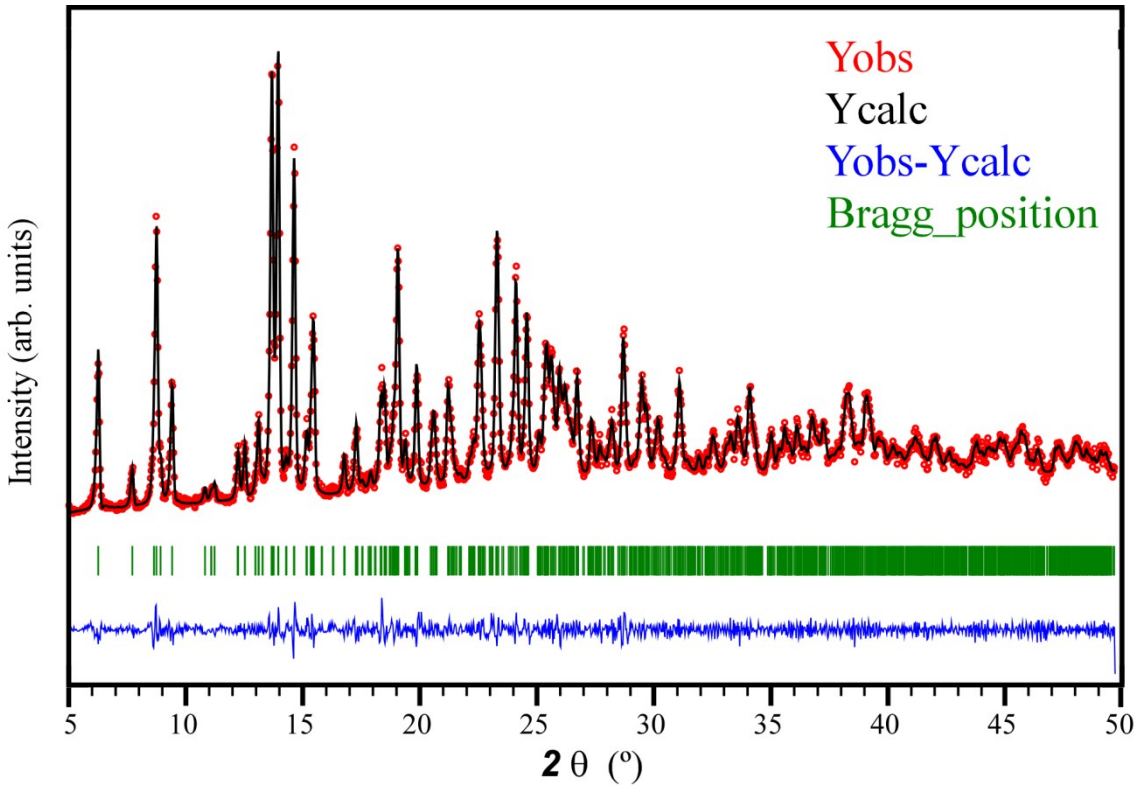

Compound 5

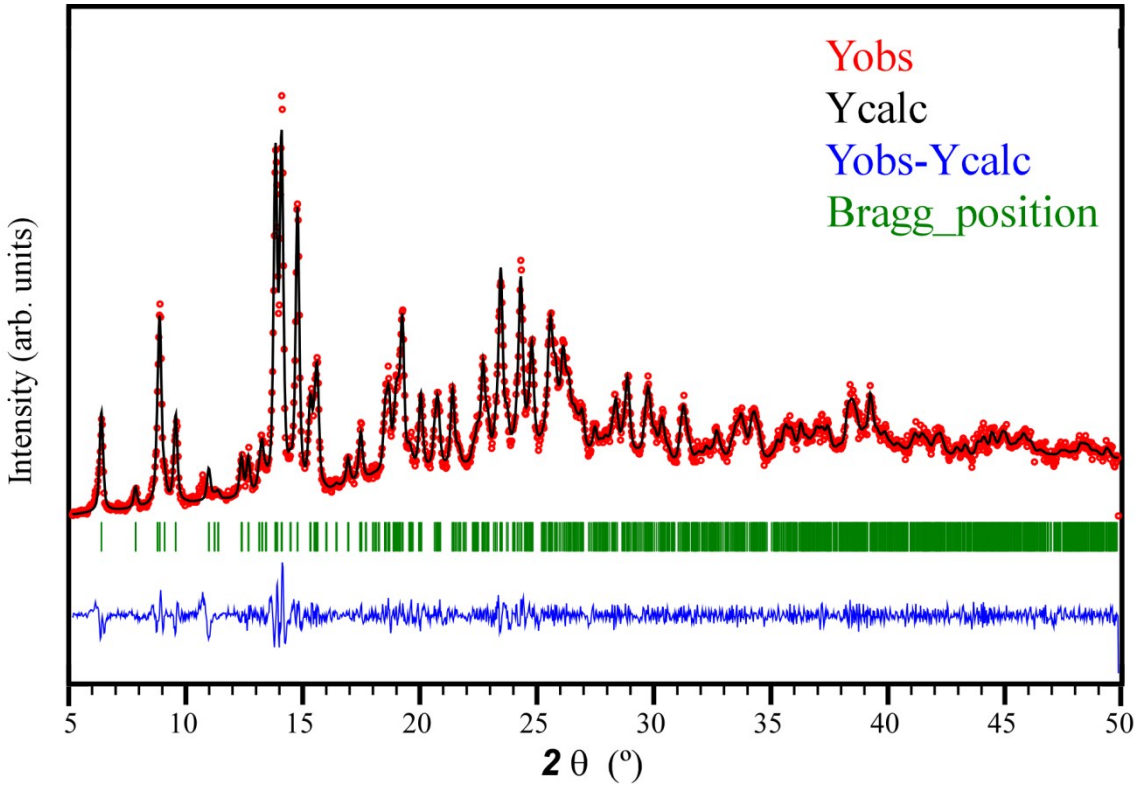

Compound 6

Figure S4. Pattern-matching analyses and experimental PXRD for complexes **5-6**.

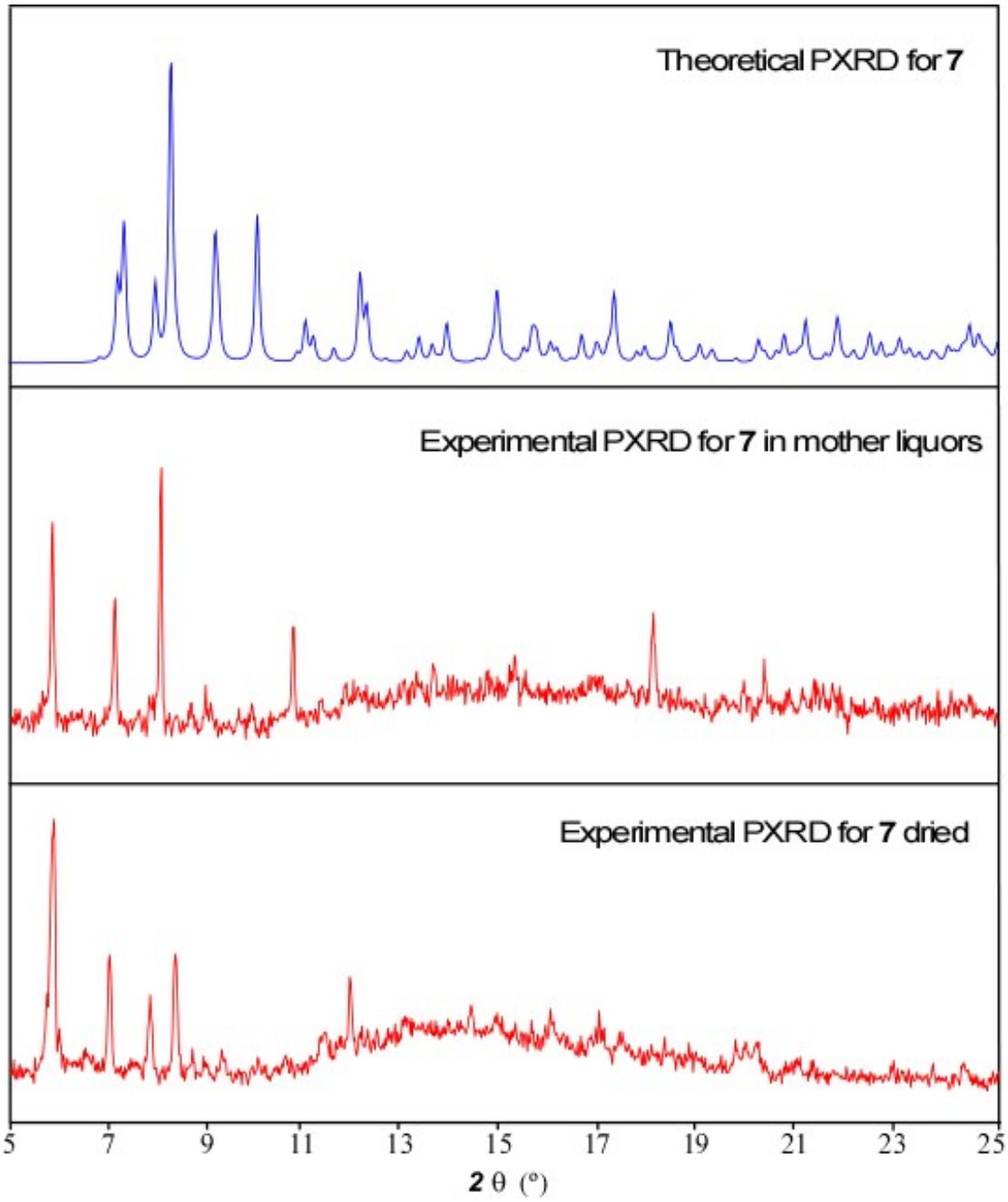

Compound 7

Figure S5. Experimental and theoretical PXRD for complex **7**. It exhibits a phase transformation due to the loss of crystallization solvent molecules. Thus, in this case, pattern-matching analysis was not performed.

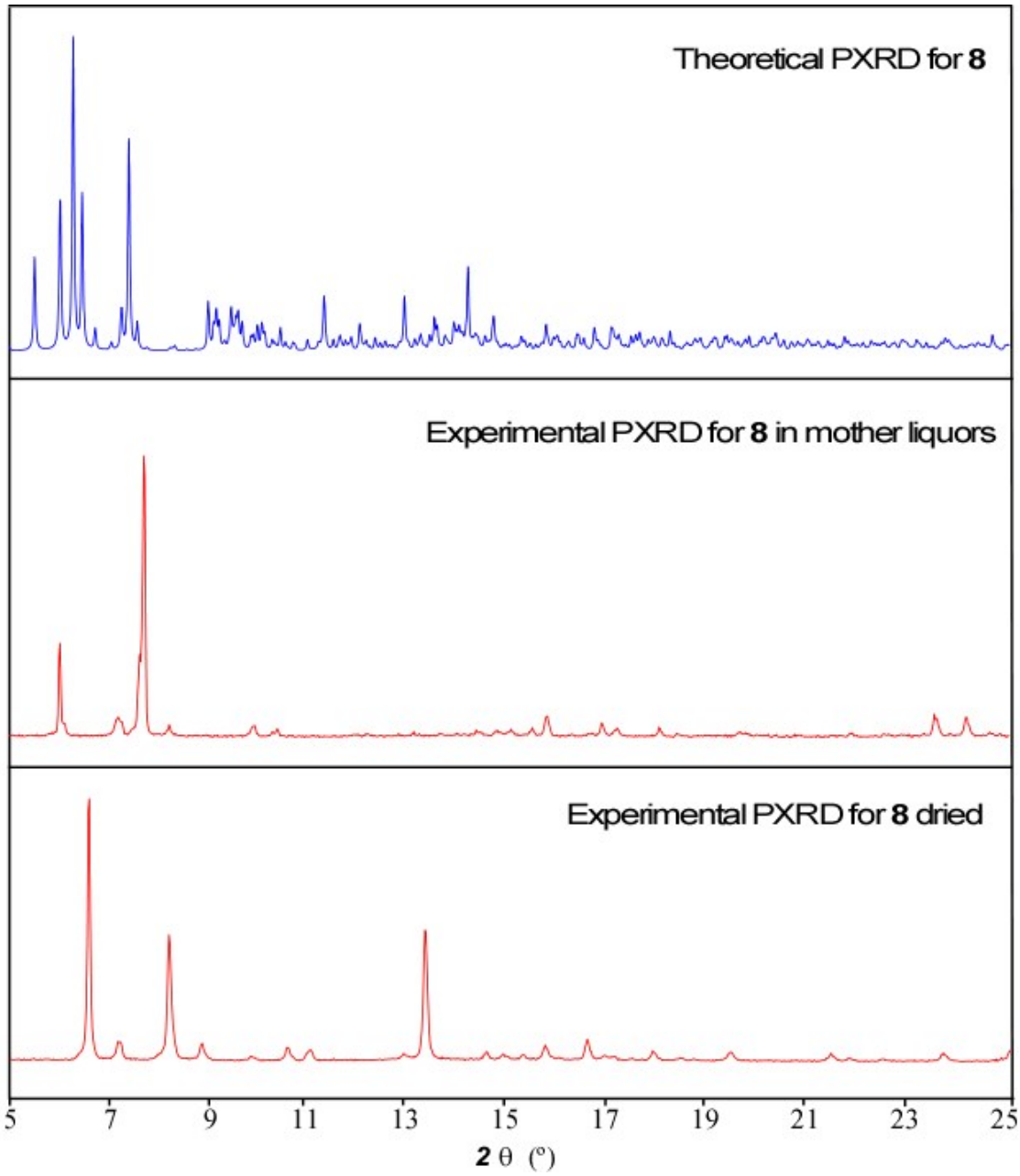

Compound 8

Figure S6. Experimental and theoretical PXRD for complex **8**. It exhibits a phase transformation due to the loss of crystallization solvent molecules. Thus, in this case, pattern-matching analysis was not performed.

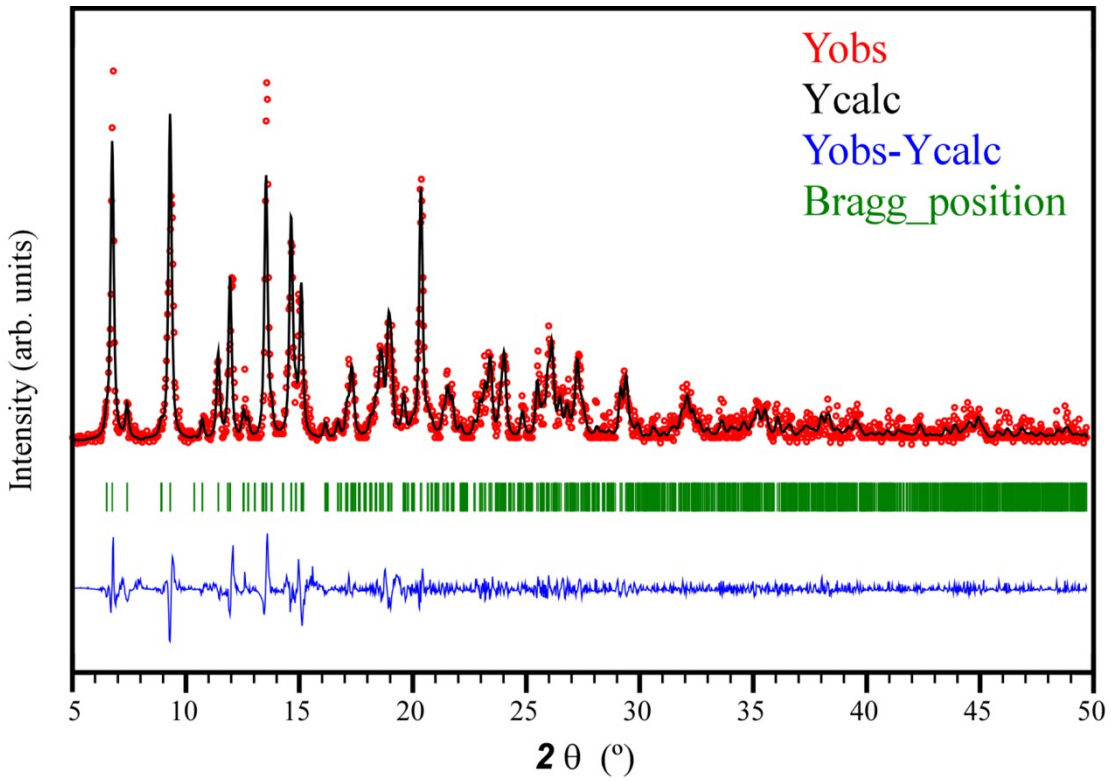

Compound 9

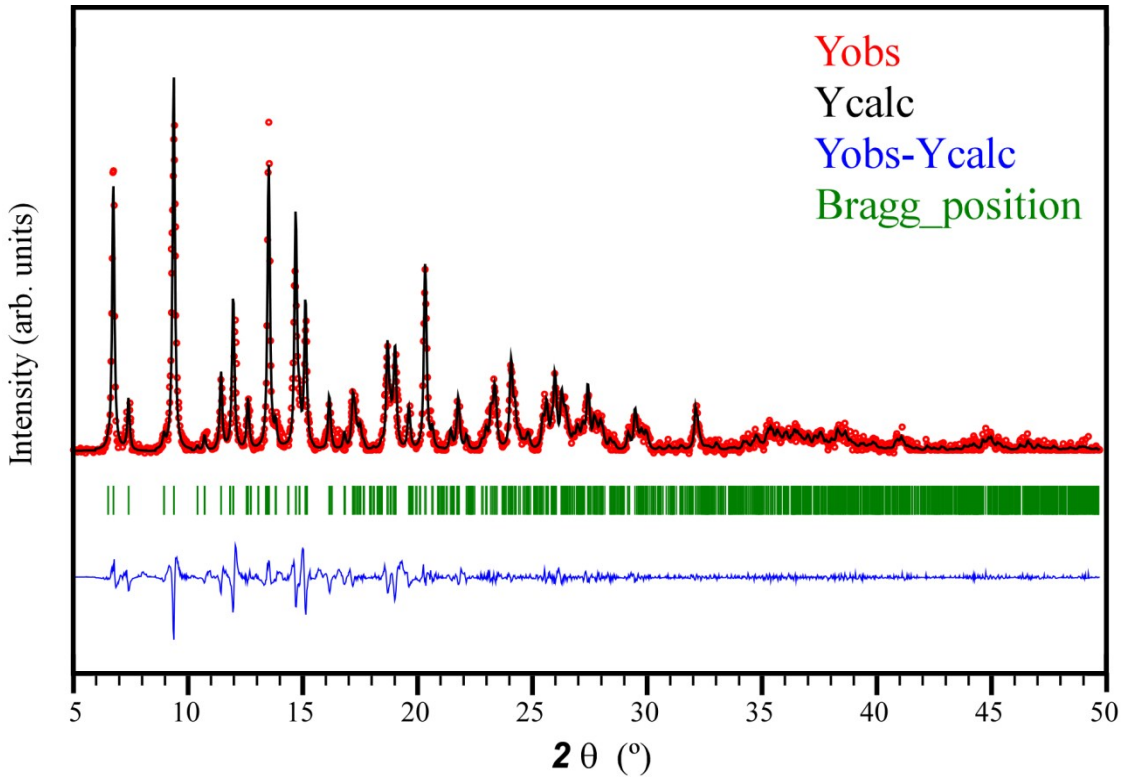

Compound 10

Figure S7. Pattern-matching analyses and experimental PXRD for complexes **9-10.**

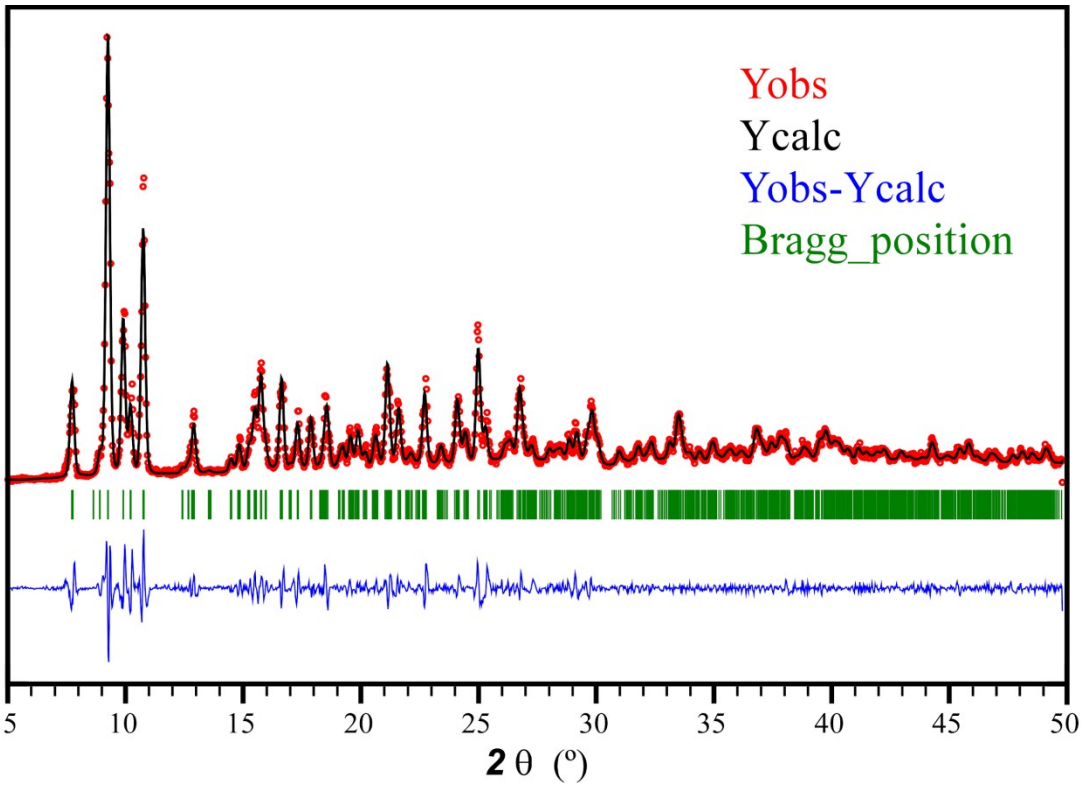

Compound 11

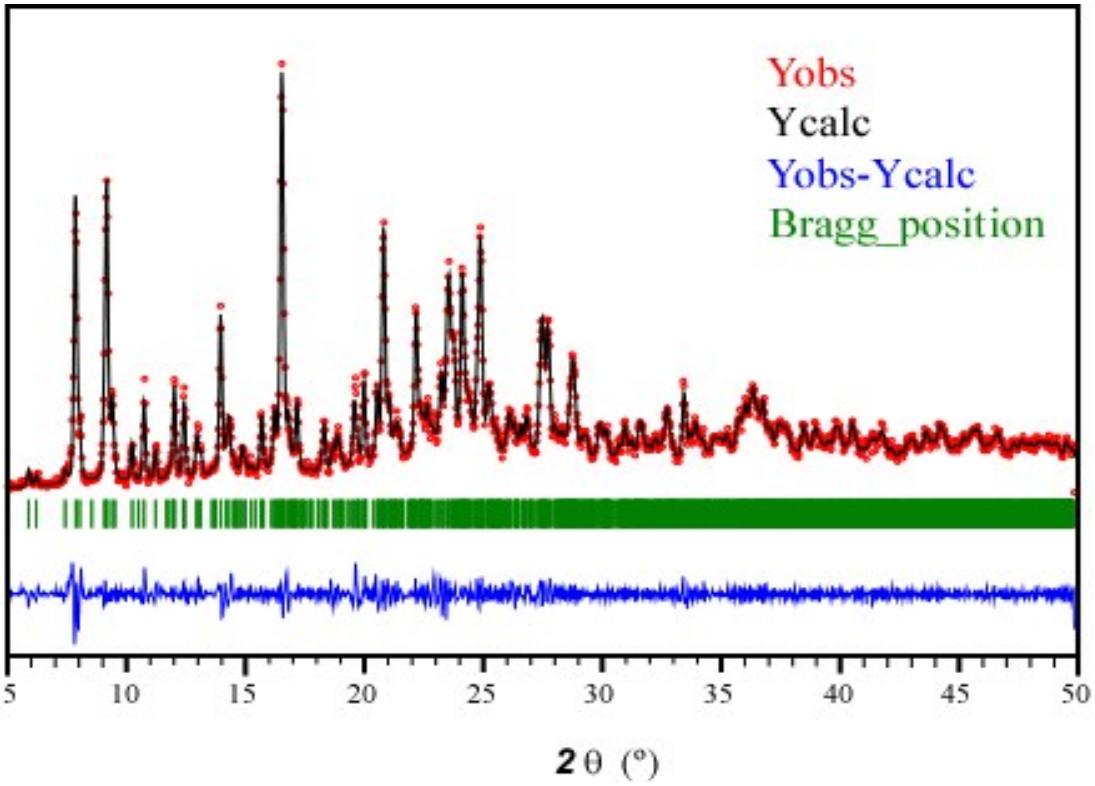

Diluted sample of Compound 3

Figure S8. Pattern-matching analyses and experimental PXRD data for complex **11** and for the diluted sample (Y/Dy = 10/1) of compound **3**.

3. Thermogravimetric measurements of compounds 7 and 8.

As stated in the manuscript, compounds **7** and **8** show solid state transformations owing to a partial loss of crystallization solvent molecules. The following thermograms confirm that both compounds preserve the tetrameric molecules in view of the similar weight loss between experimental and calculated values. Polycrystalline sample of compound **7**, once it transforms, is described with the $[Zn_2Dy_2(\mu_3\text{-}L')_2(\mu\text{-}sal)_2(NO_3)(CH_3OH)]NO_3{\cdot}2CH_3OH$ formula on the basis of the first mass loss (accounting for solely 2 crystallization MeOH molecules; calc. %3.14, exp. %3.52) and the weight of the residue (calc. %26.31, exp. %26.45). As a consequence, it may be stated that the solid state transformation causes the release of 3 crystallization methanol molecules.

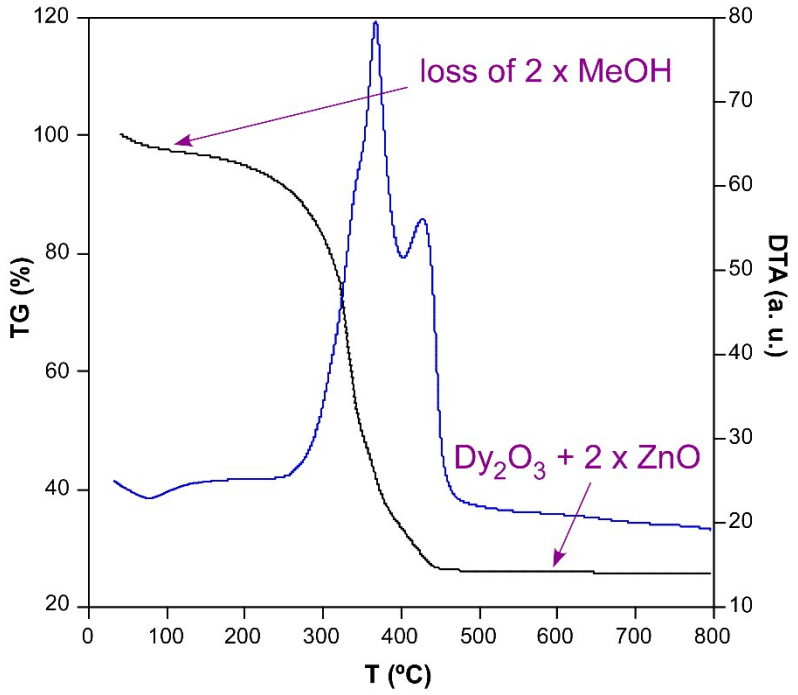

Figure S9. Thermogravimetric analysis of compound **7**.

On its part, polycrystalline sample of compound **8** is more accurately described with the $[Zn_2Er_2(\mu_3\text{-}L')_2(\mu\text{-}sal)_2(CH_3OH)_2](NO_3)_2{\cdot}2CH_3OH$ chemical formula on the basis of the first mass loss (accounting for solely 2 crystallization MeOH molecules; calc. %3.08, exp. %2.92) and the weight of the residue (calc. %26.13, exp. %26.05). As a consequence, it may be stated that the solid state transformation causes the release of 2 crystallization methanol molecules.

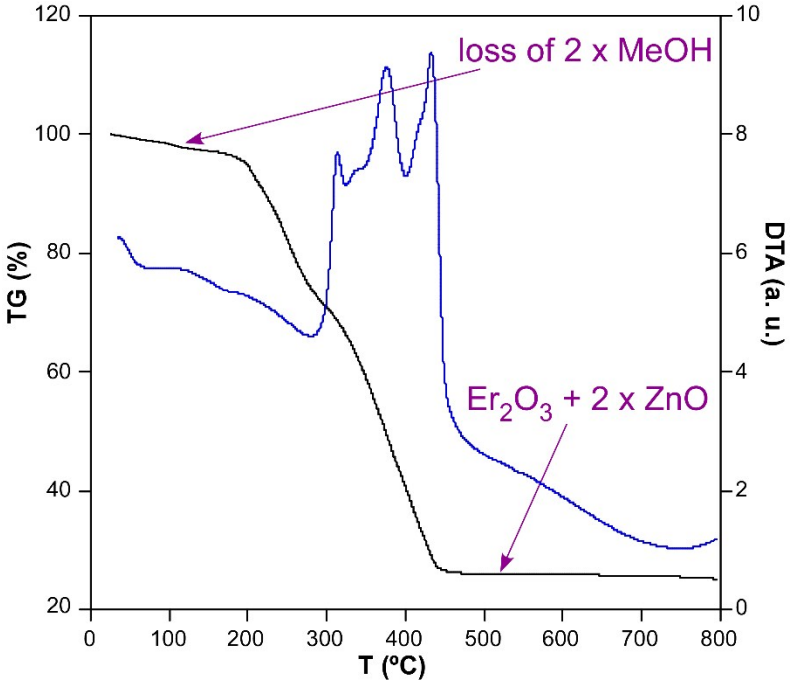

Figure S10. Thermogravimetric analysis of compound **8**.

4. ORTEP views.

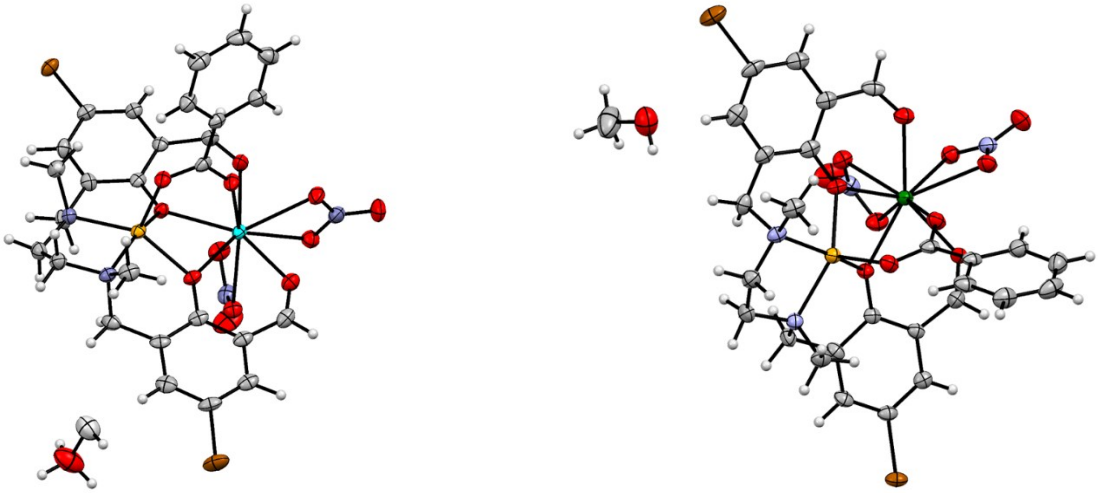

Figure S11. ORTEP views for complex **1** (left) and **2** (right).

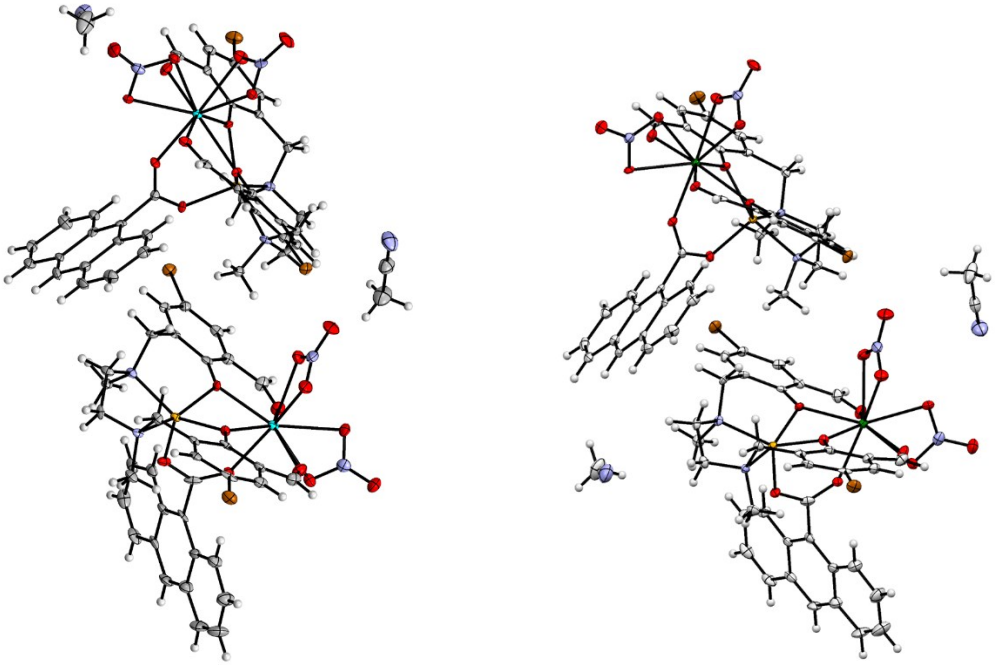

Figure S12. ORTEP views for complex **3** (left) and **4** (right).

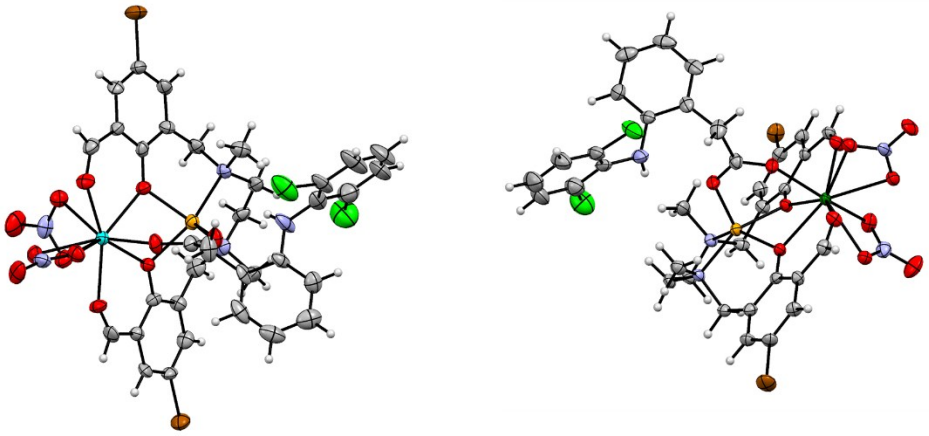

Figure S13. ORTEP views for complex **5** (left) and **6** (right).

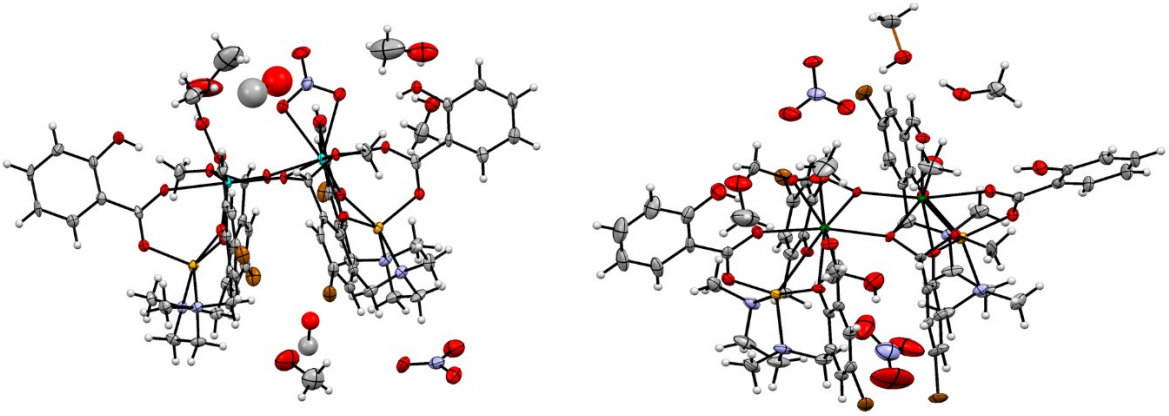

Figure S14. ORTEP views for complex **7** (left) and **8** (right).

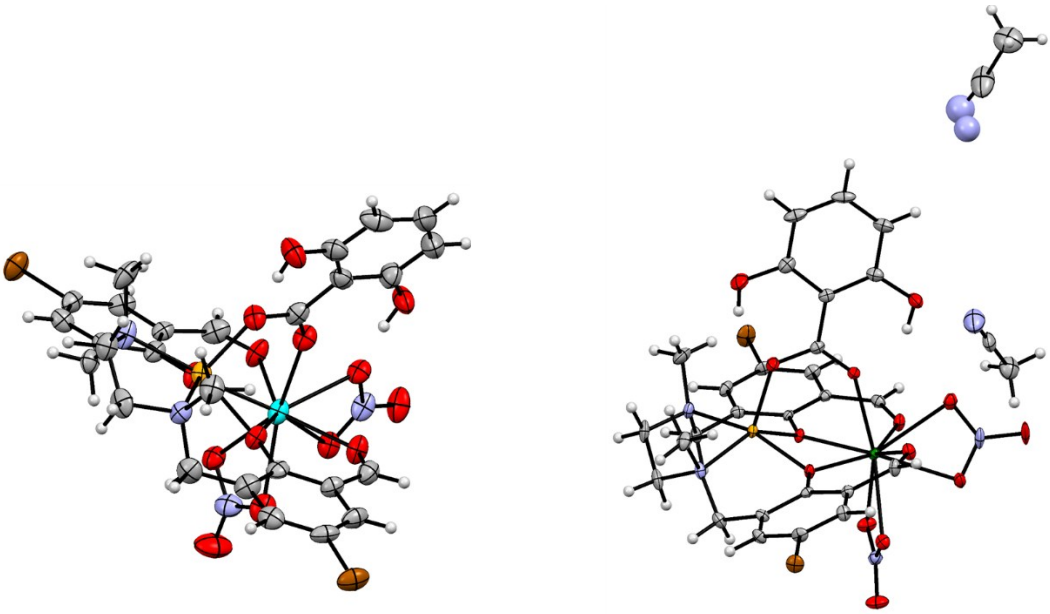

Figure S15. ORTEP views for complex **10** (left) and **11** (right).

5. Representation of the main intermolecular interactions.

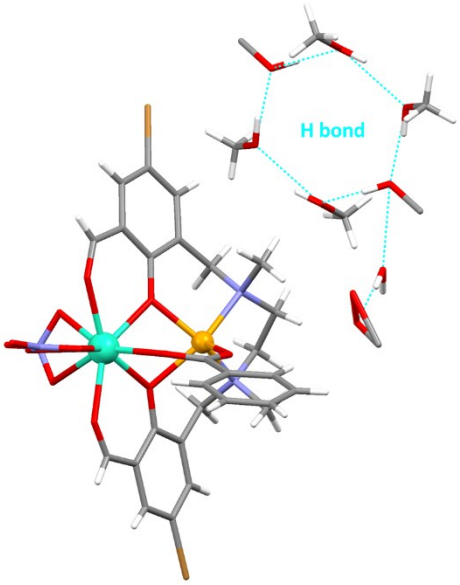

Compound 1-2

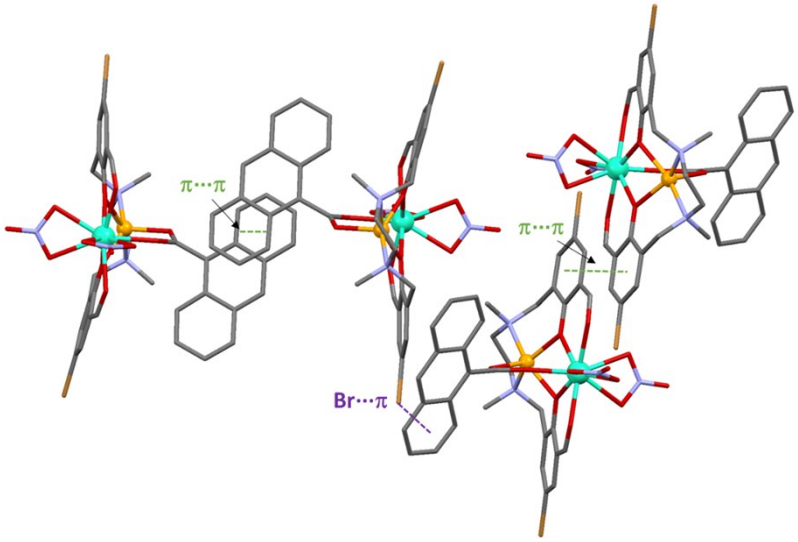

Compound 3-4

Figure S16. The most representative intermolecular interactions and packing modes for complexes **1-2** (up) and **3-4** (down). H bonds, π···π and Br···π interactions are shown with dashed blue, green and purple lines, respectively.

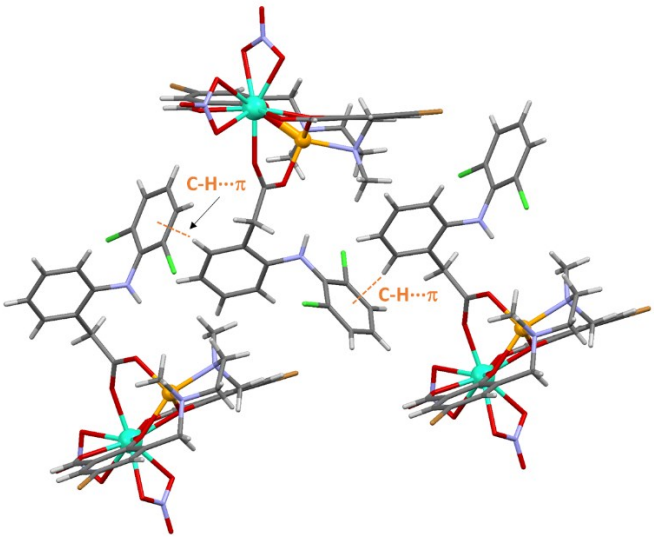

Compound 5-6

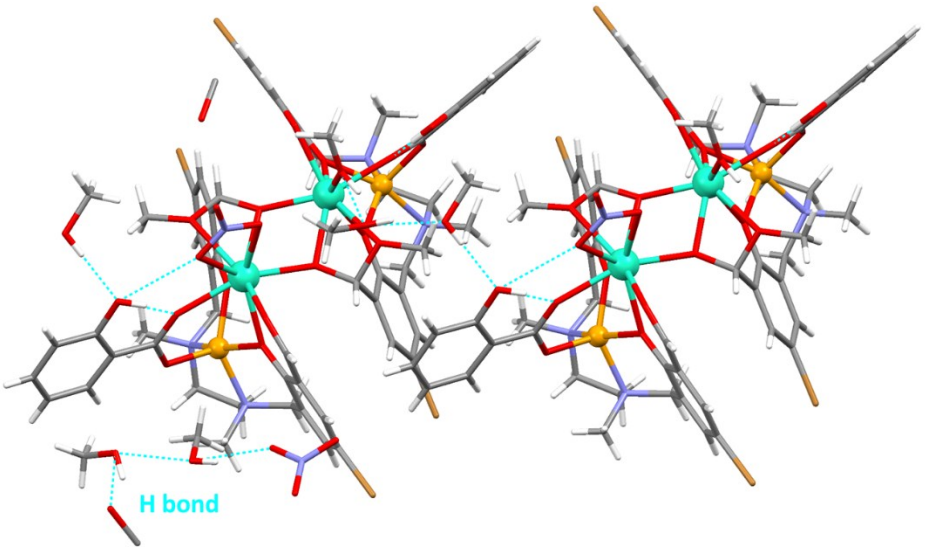

Compound 7

Figure S17. The most representative intermolecular interactions and packing modes for complexes **5-6** (up) and **7** (down). H bonds, and C-H···π interactions are shown with dashed blue and orange lines, respectively.

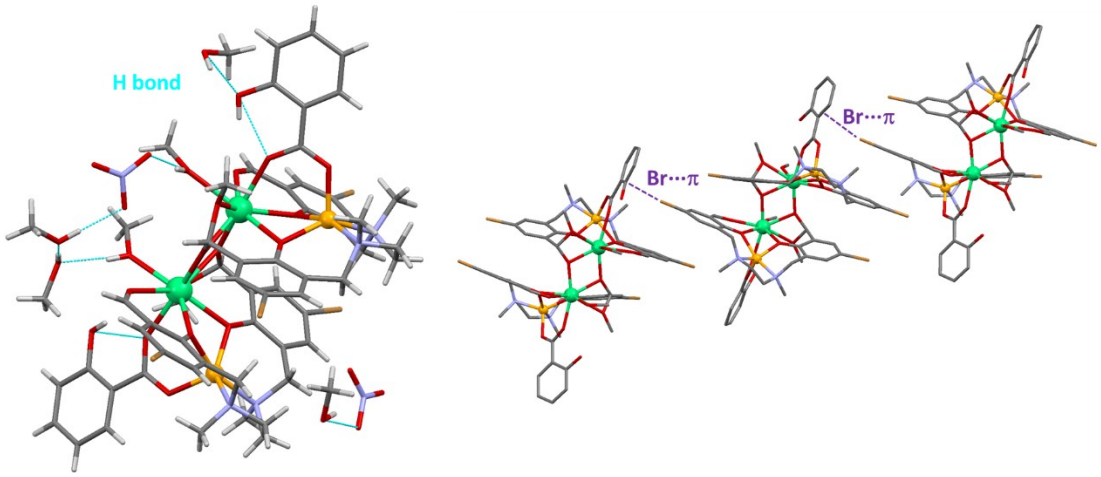

Compound 8

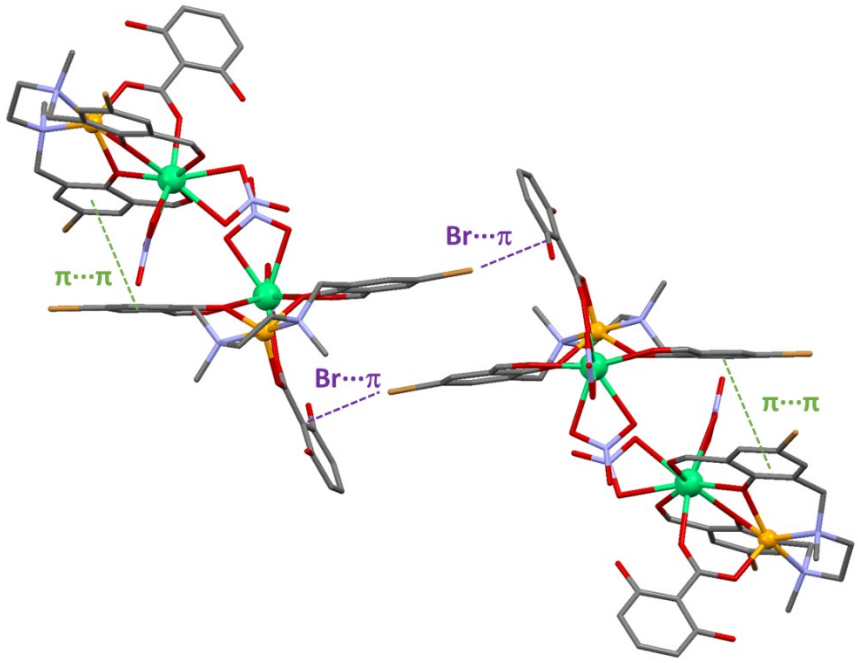

Compound 9-10

Figure S18. The most representative intermolecular interactions and packing modes for complexes **8** (up) and **9-10** (down). H bonds, π···π and Br···π interactions are shown with dashed blue, green and purple lines, respectively.

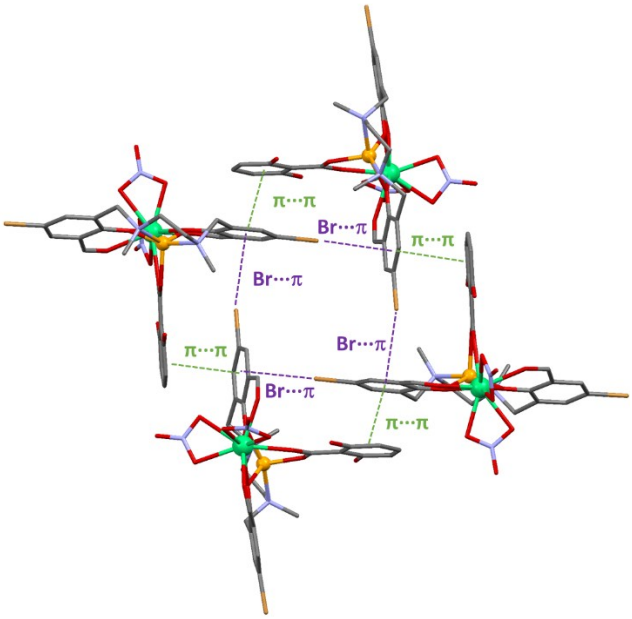

Compound 11

Figure S19. The most representative intermolecular interactions and packing modes for complex **11**. π···π and Br···π interactions are shown with dashed green and purple lines, respectively.

6. Continuous Shape Measurements.

Table S3. Continuous Shape Measurements for the ZnN_2O_3 coordination environment.

PP-5	1 D5h	Pentagon
VOC-5	2 C4v	Vacant octahedron
TBPY-5	3 D3h	Trigonal bipyramid
SPY-5	4 C4v	Spherical square pyramid
JTBPY-5	5 D3h	Johnson trigonal bipyramid J12

Complex	PP-5	VOC-5	TBPY-5	SPY-5	JTBPY-5
1	31.845	1.839	3.621	**0.454**	5.971
2	31.727	1.868	3.700	**0.458**	6.041
3-Zn1	30.628	1.704	3.734	**0.417**	6.286
3-Zn2	31.805	1.786	3.278	**0.540**	5.836
4-Zn1	30.614	1.692	3.790	**0.420**	6.341
4-Zn2	31.898	1.756	3.332	**0.542**	5.854
5	32.116	2.117	3.340	**0.452**	5.782
6	31.936	2.189	3.356	**0.476**	5.810
7-Zn1	31.751	2.381	2.651	**0.927**	4.982
7-Zn2	31.972	2.084	2.818	**0.876**	4.822
8-Zn1	32.133	2.508	2.559	**0.942**	4.906
8-Zn2	32.187	2.571	2.539	**0.939**	4.804
10	31.721	1.788	3.669	**0.444**	5.859
11	29.280	2.149	3.050	**1.058**	5.395

Table S4. Continuous Shape Measurements for the LnO_9 coordination environment.

EP-9	1 D9h	Enneagon
OPY-9	2 C8v	Octagonal pyramid
HBPY-9	3 D7h	Heptagonal bipyramid
JTC-9	4 C3v	Johnson triangular cupola J3
JCCU-9	5 C4v	Capped cube J8
CCU-9	6 C4v	Spherical-relaxed capped cube
JCSAPR-9	7 C4v	Capped square antiprism J10
CSAPR-9	8 C4v	Spherical capped square antiprism
JTCTPR-9	9 D3h	Tricapped trigonal prism J51
TCTPR-9	10 D3h	Spherical tricapped trigonal prism
JTDIC-9	11 C3v	Tridiminished icosahedron J63
HH-9	12 C2v	Hula-hoop
MFF-9	13 Cs	Muffin

Complex	JCSAPR-9	CSAPR-9	JTCTPR-9	TCTPR-9	MFF-9
1	2.017	**1.255**	3.017	1.702	1.515
2	1.936	**1.212**	2.903	1.656	1.483
3-Dy1	1.750	**1.019**	3.371	2.060	1.511
3-Dy2	1.980	**1.316**	3.174	1.833	1.463
4-Er1	1.871	**1.194**	3.081	1.722	1.390
4-Er2	1.686	**0.987**	3.303	2.015	1.479
5	1.818	**1.053**	3.681	2.150	1.221
6	1.738	**1.028**	3.486	2.204	1.230
7-Dy1	2.705	1.991	2.924	**1.720**	2.088
10	1.558	**0.896**	3.445	2.138	1.255
11	1.797	**1.222**	2.548	1.713	1.555

Table S5. Continuous Shape Measurements for the LnO_8 coordination environment.

OP-8	1 D8h	Octagon
HPY-8	2 C7v	Heptagonal pyramid
HBPY-8	3 D6h	Hexagonal bipyramid
CU-8	4 Oh	Cube
SAPR-8	5 D4d	Square antiprism
TDD-8	6 D2d	Triangular dodecahedron
JGBF-8	7 D2d	Johnson - Gyrobifastigium (J26)
JETBPY-8	8 D3h	Johnson - Elongated triangular bipyramid (J14)
JBTP-8	9 C2v	Johnson - Biaugmented trigonal prism (J50)
BTPR-8	10 C2v	Biaugmented trigonal prism
JSD-8	11 D2d	Snub disphenoid (J84)
TT-8	12 Td	Triakis tetrahedron
ETBPY-8	13 D3h	Elongated trigonal bipyramid

Complex	SAPR-8	TDD-8	JBTPR-8	BTPR-8	JSD-8
7-Dy2	5.848	3.691	3.907	**3.386**	4.353
8-Er1	4.354	**2.201**	2.863	2.315	3.205
8-Er2	4.621	**2.496**	2.970	2.656	3.154

7. Magnetic properties.

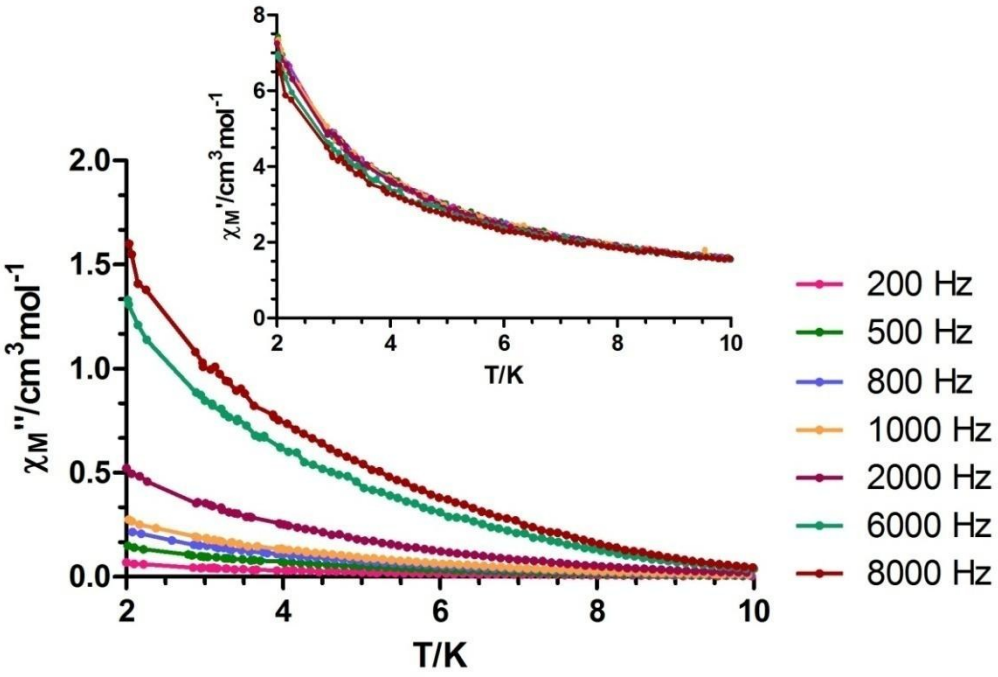

Figure S20. Temperature dependence of in-phase (inset) and out-of-phase components of the *ac* susceptibility in the absence of an external field for **1**.

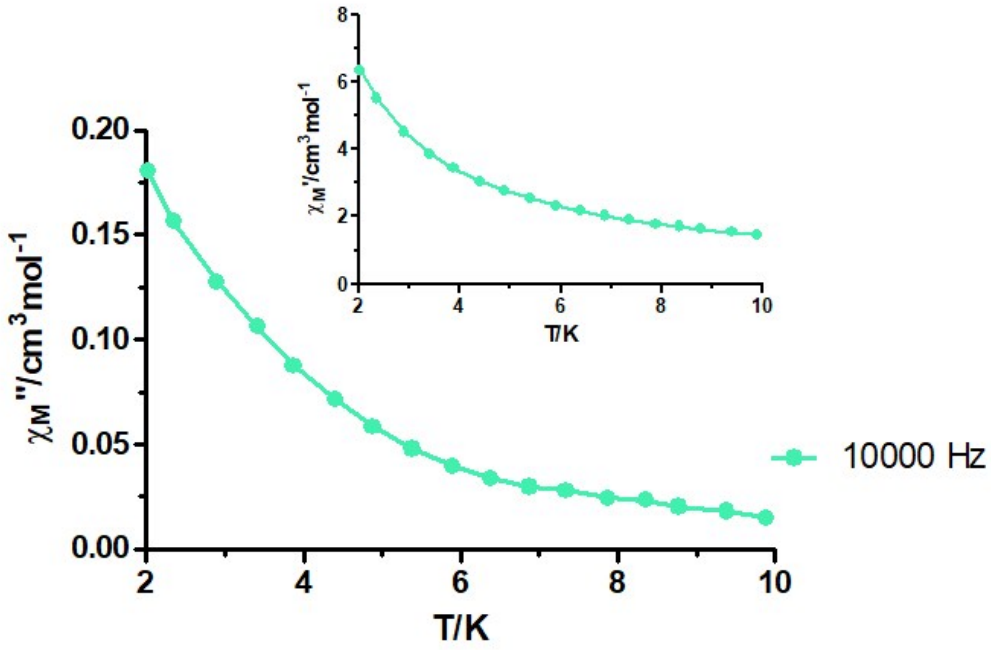

Figure S21. Temperature dependence of in-phase (inset) and out-of-phase components of the *ac* susceptibility in the absence of an external field for **3**.

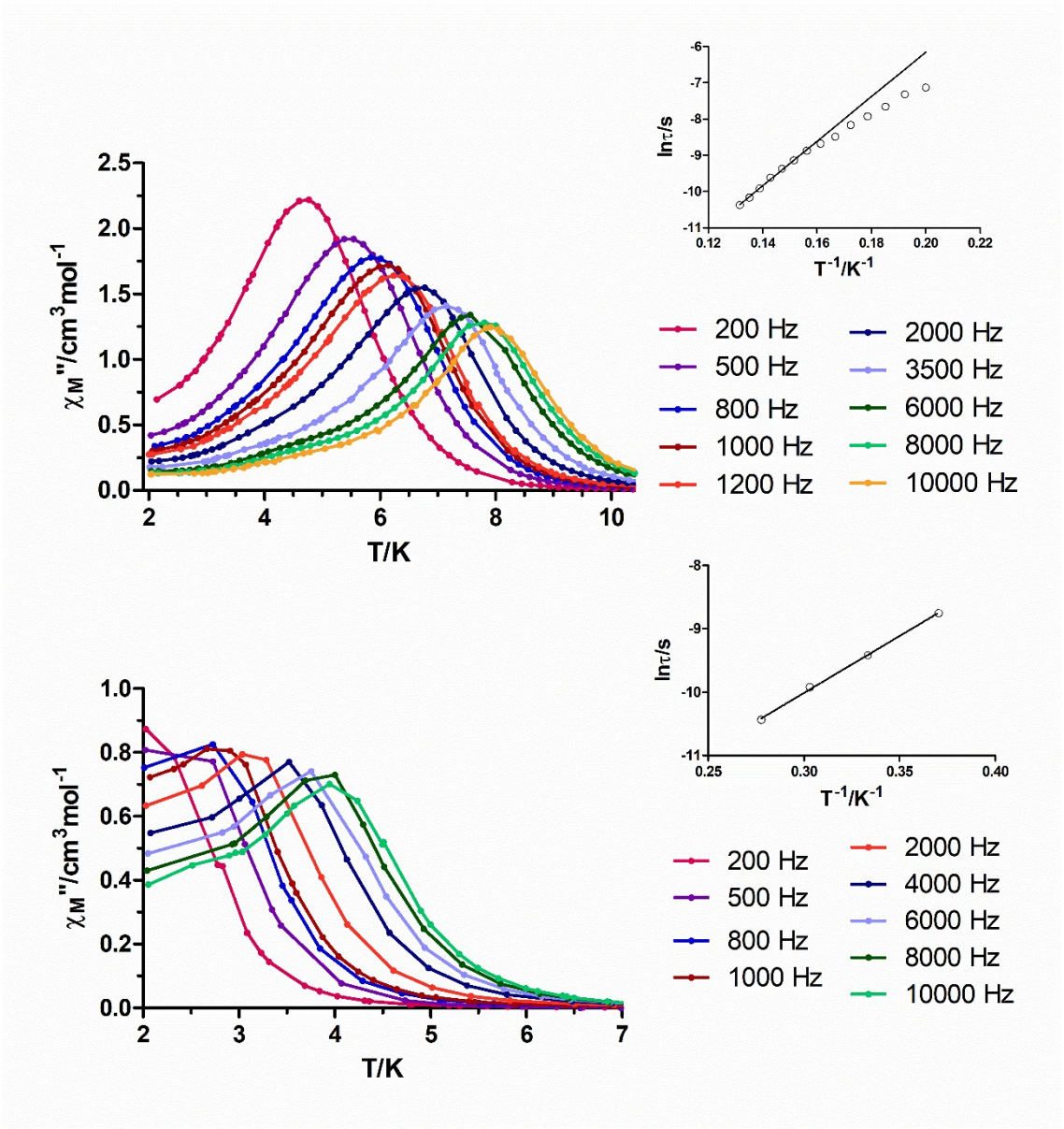

Figure S22. Temperature dependence of out-of-phase components of the *ac* susceptibility in a *dc* applied field of 1000 Oe for **1** (up) and **2** (bottom). Insets: Arrhenius plots for **1** (up) and **2** (bottom). The black line accounts for the best fit to Orbach relaxation mode.

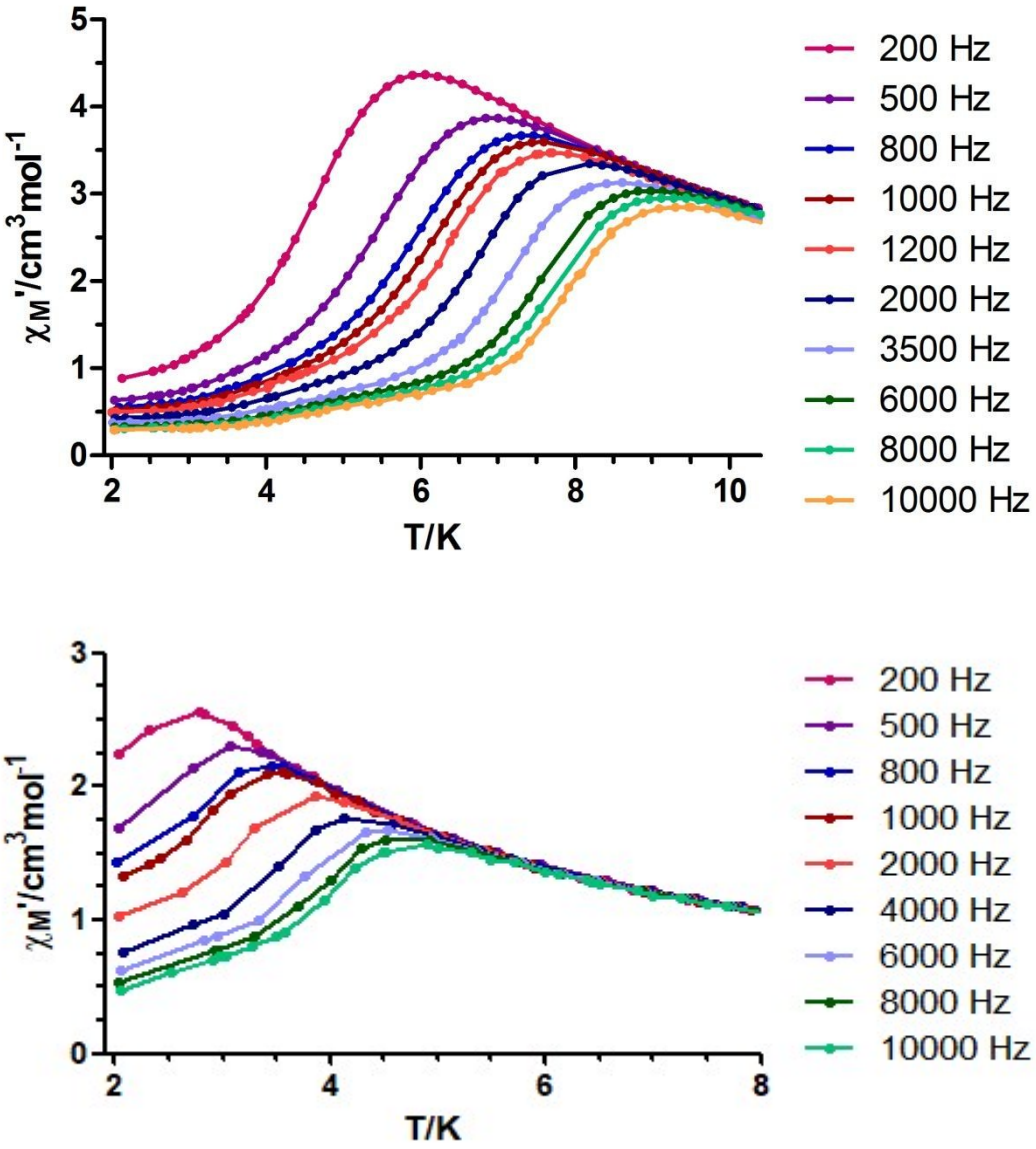

Figure S23. Temperature dependence of in-phase components of the *ac* susceptibility in a *dc* applied field of 1000 Oe for **1** (up) and **2** (bottom).

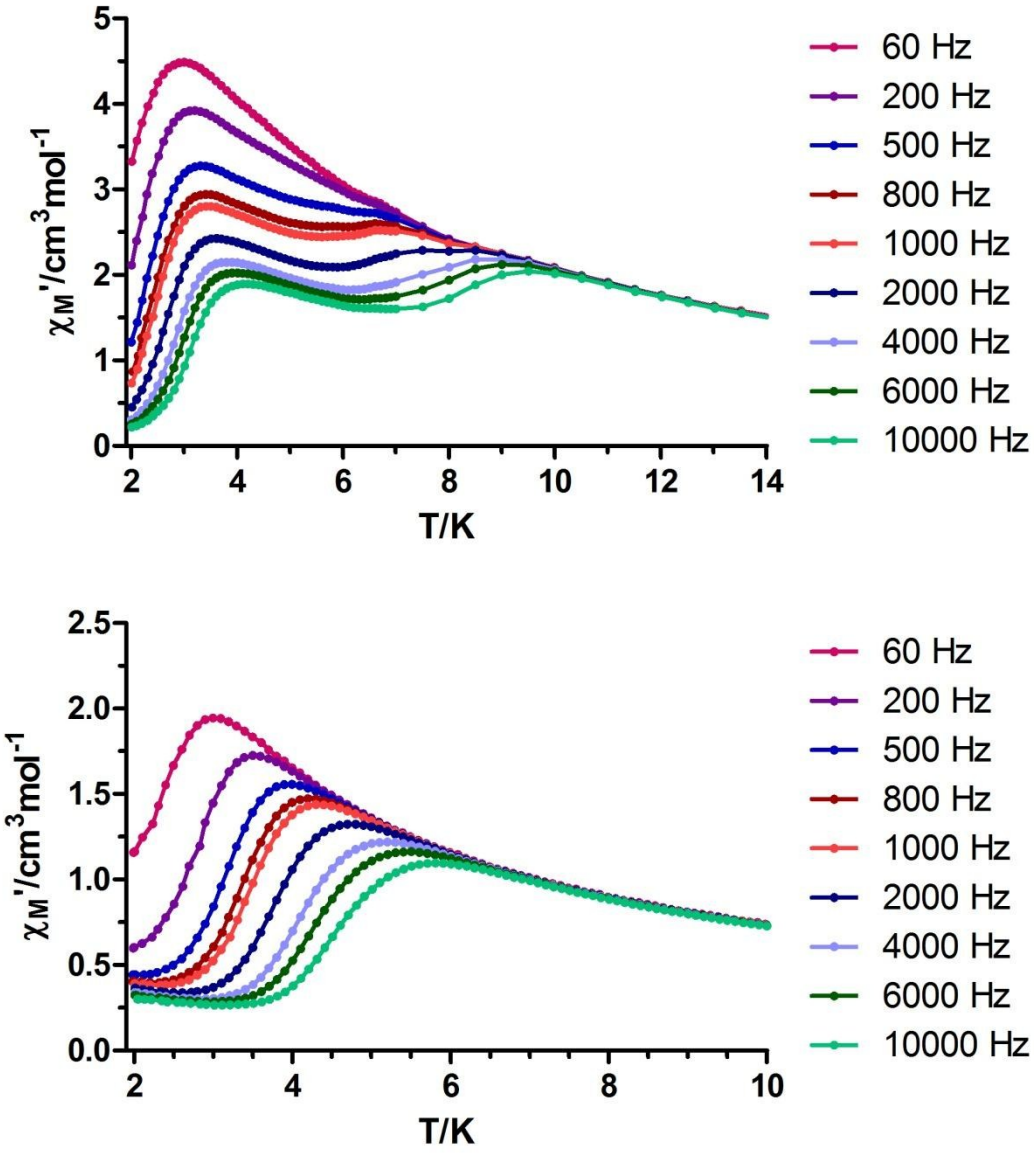

Figure S24. Temperature dependence of in-phase components of the *ac* susceptibility in a *dc* applied field of 1000 Oe for **3** (up) and **4** (bottom).

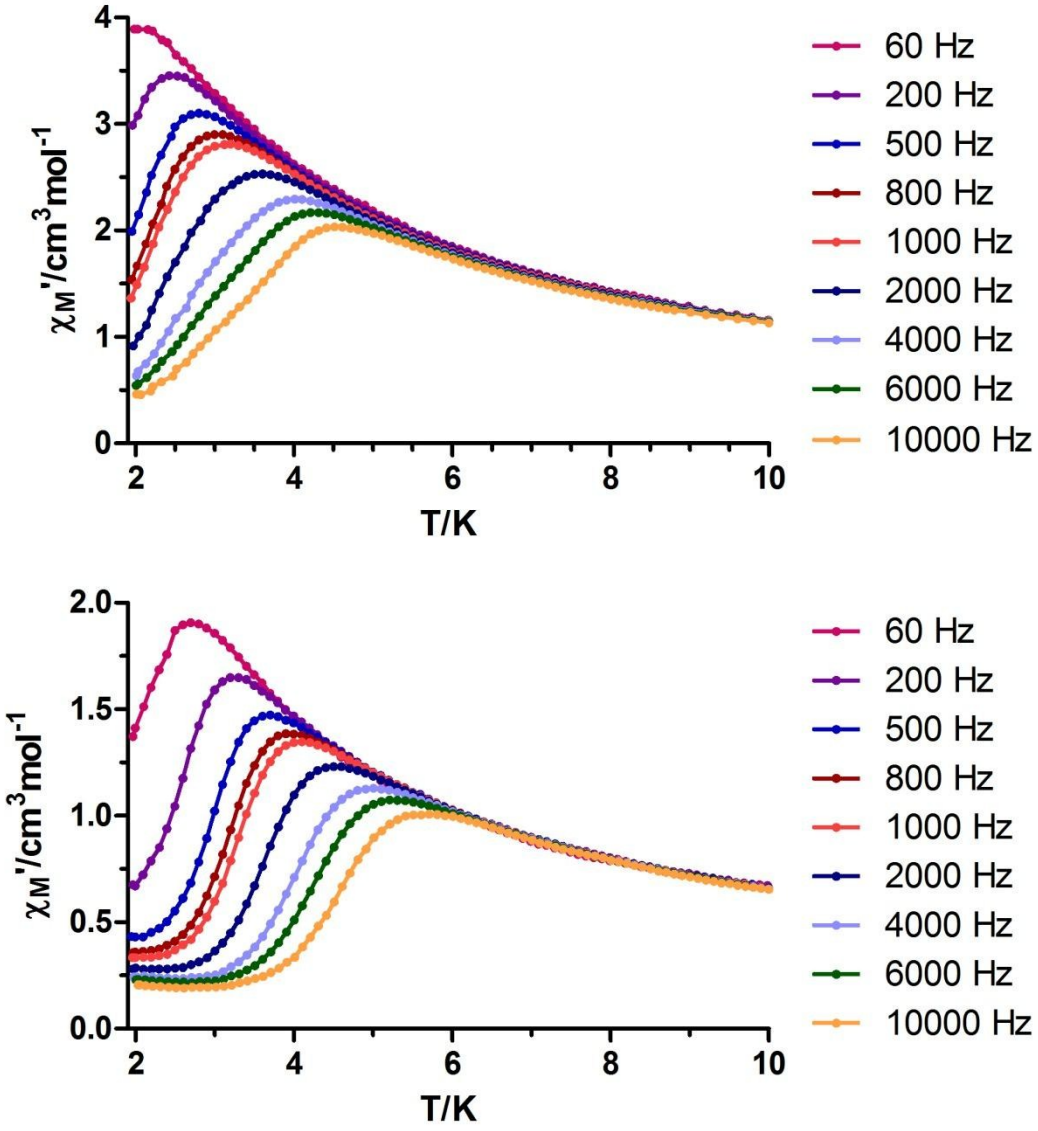

Figure S25. Temperature dependence of in-phase components of the *ac* susceptibility in a *dc* applied field of 1000 Oe for **5** (up) and **6** (bottom).

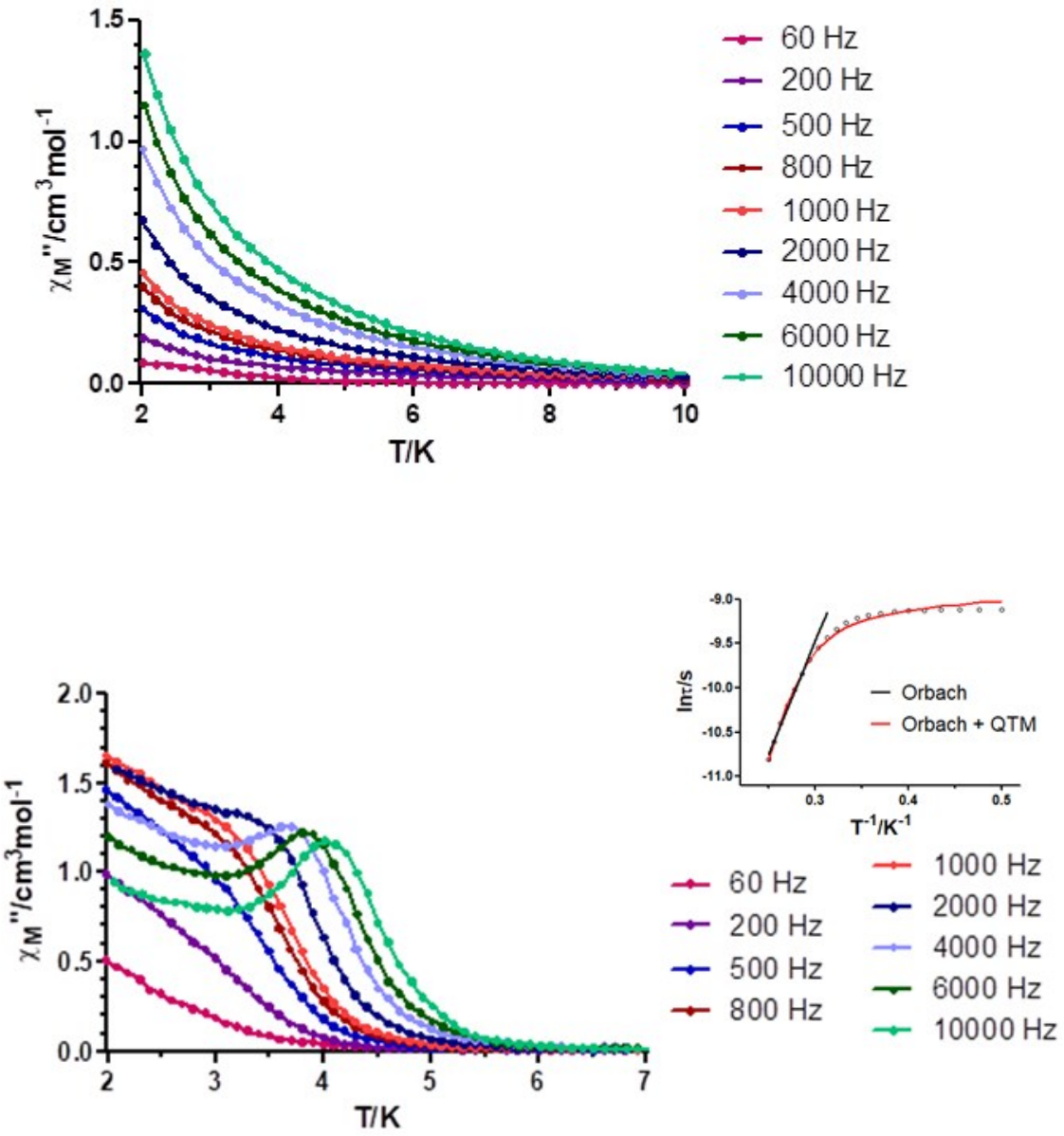

Figure S26. Temperature dependence of out-of-phase components of the *ac* susceptibility in a *dc* applied field of 1000 Oe for **7** (up) and **8** (bottom). Inset: Arrhenius plots for **8**. The black line accounts for the best fit considering Orbach relaxation, and the red line corresponds to Orbach plus QTM relaxation.

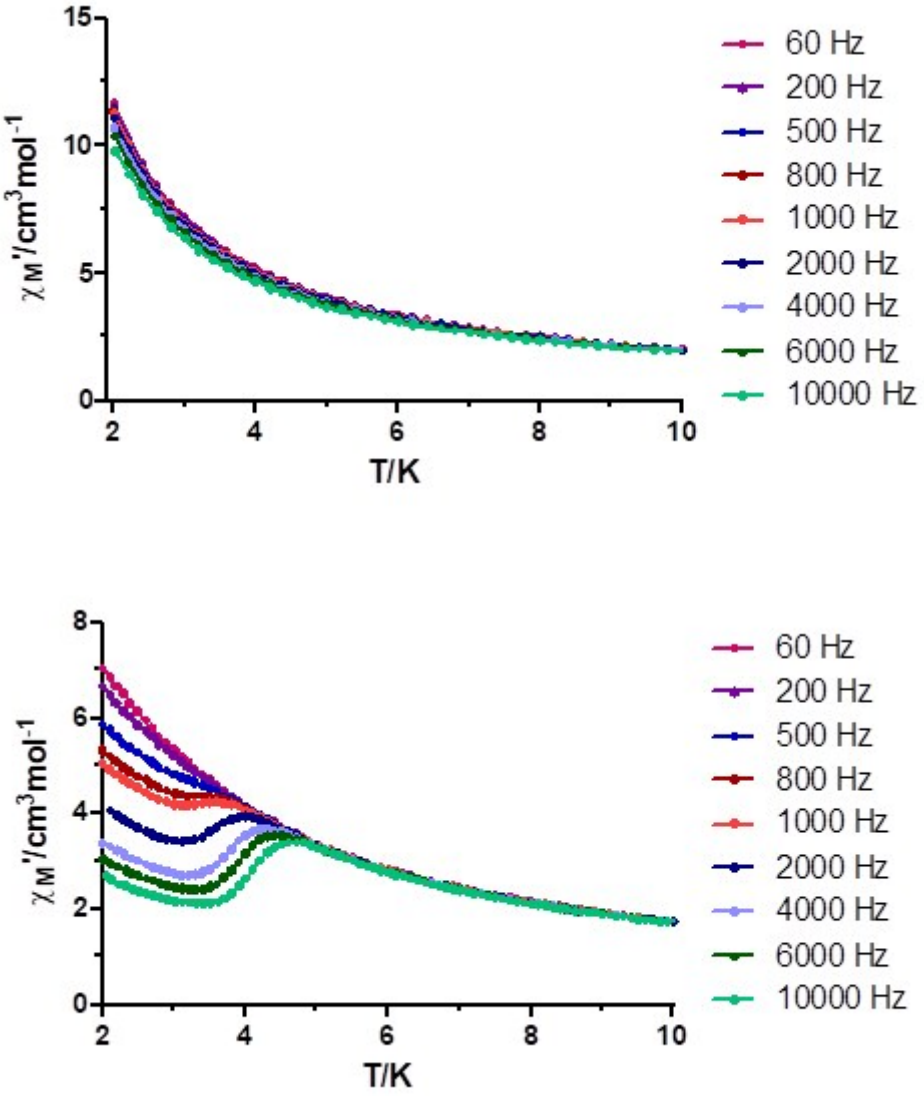

Figure S27. Temperature dependence of in-phase components of the *ac* susceptibility in a *dc* applied field of 1000 Oe for **7** (up) and **8** (bottom).

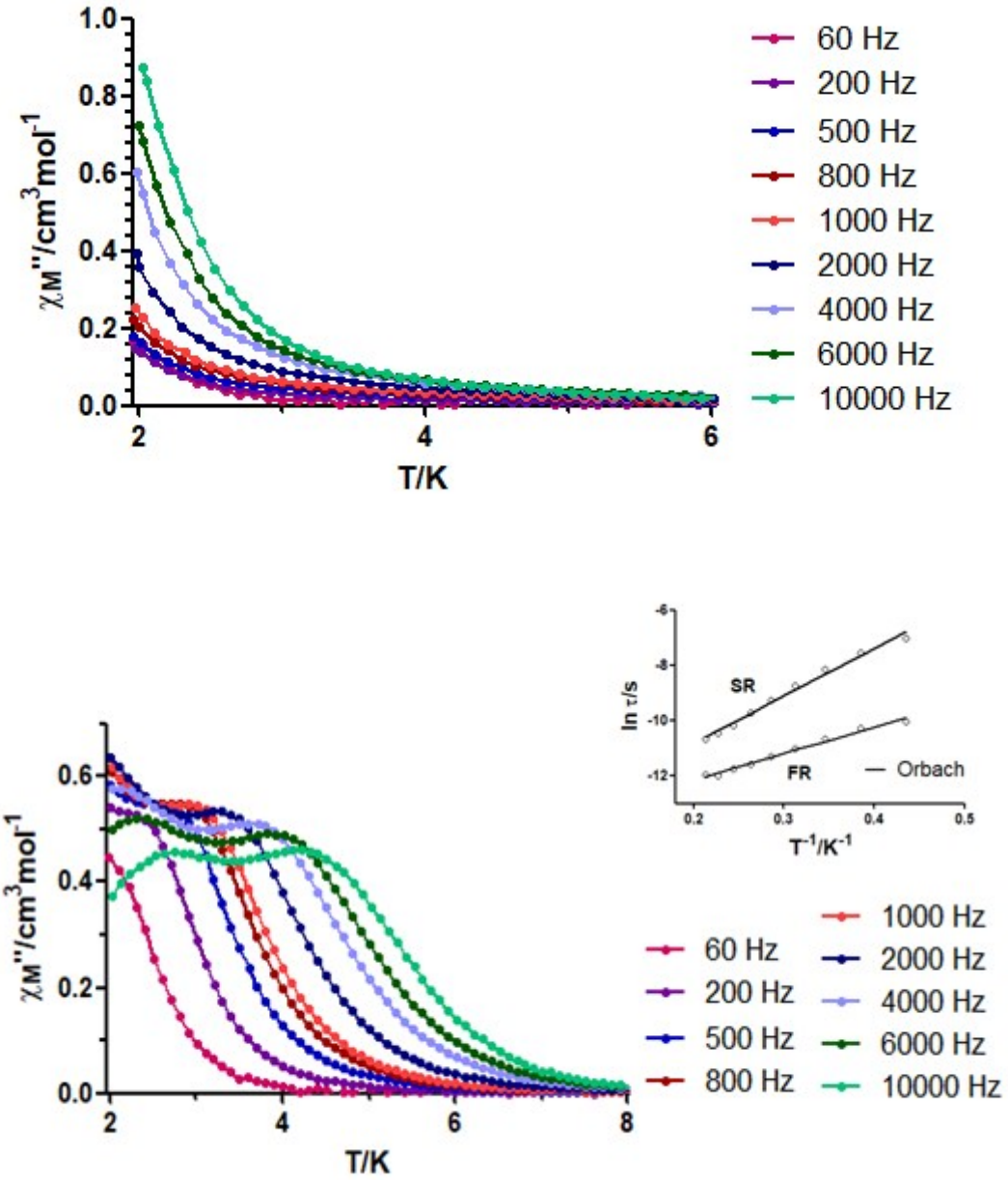

Figure S28. Temperature dependence of out-of-phase components of the *ac* susceptibility in a *dc* applied field of 1000 Oe for **9** (up) and **10** (bottom). Inset: Arrhenius plot for **10**. The black line accounts for the best fit considering Orbach relaxation.

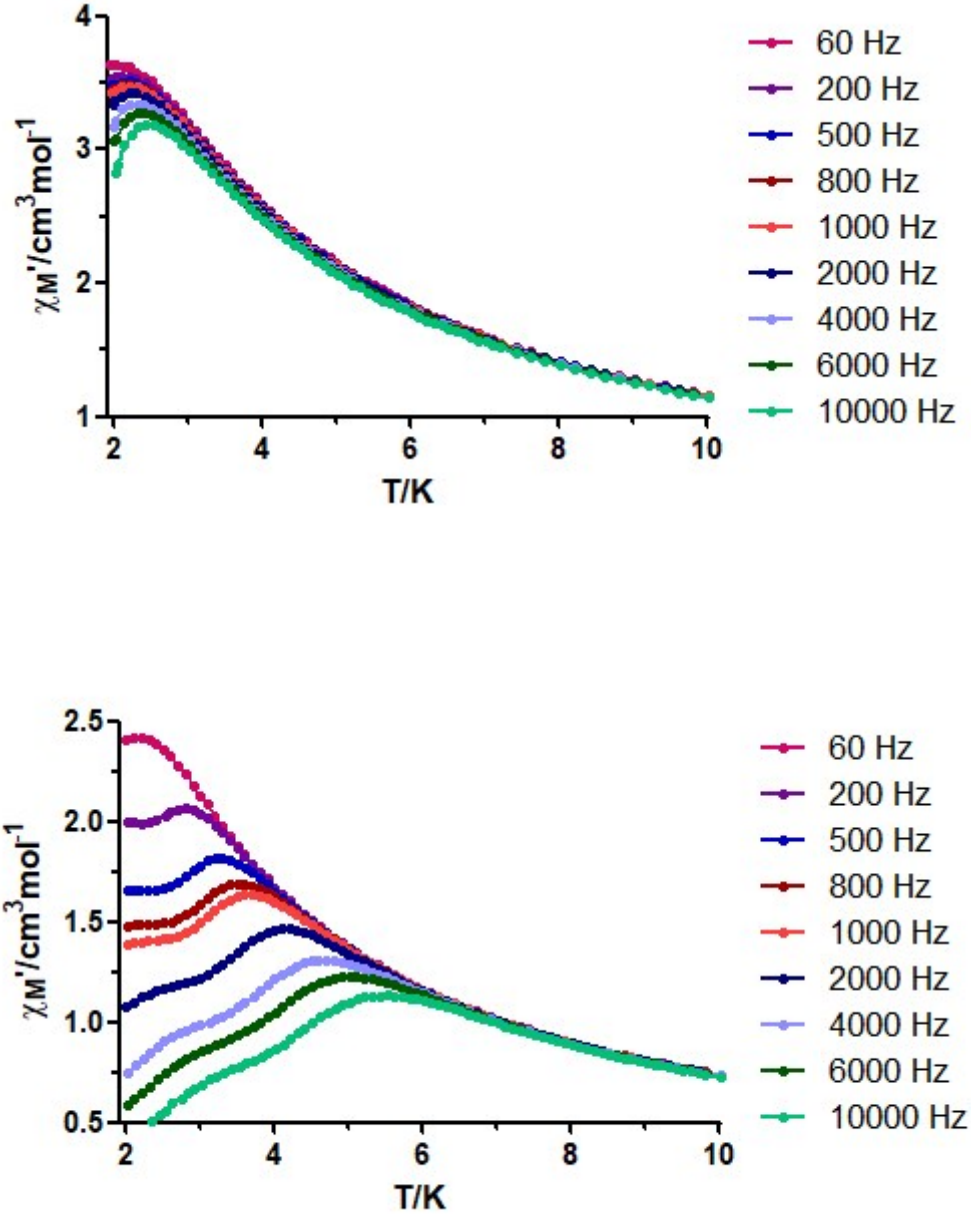

Figure S29. Temperature dependence of in-phase components of the *ac* susceptibility in a *dc* applied field of 1000 Oe for **9** (up) and **10** (bottom).

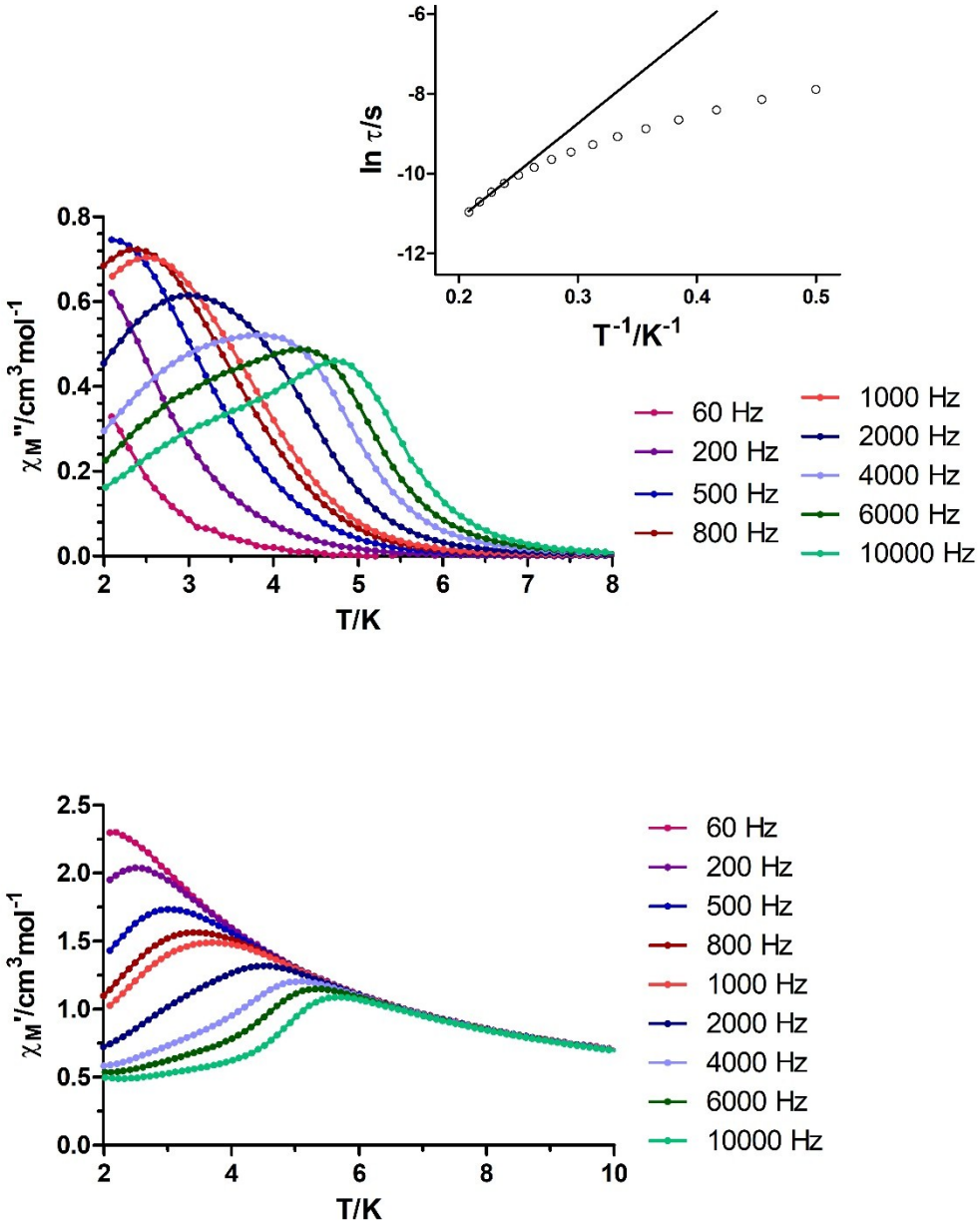

Figure S30. Temperature dependence of out-of-phase (up) and in-phase (bottom) components of the *ac* susceptibility in a *dc* applied field of 1000 Oe for **11** (up). Inset: Arrhenius plots for **11**. The black line accounts for the best fit considering Orbach relaxation, and the red line correspond to Orbach plus Raman plus QTM relaxation.

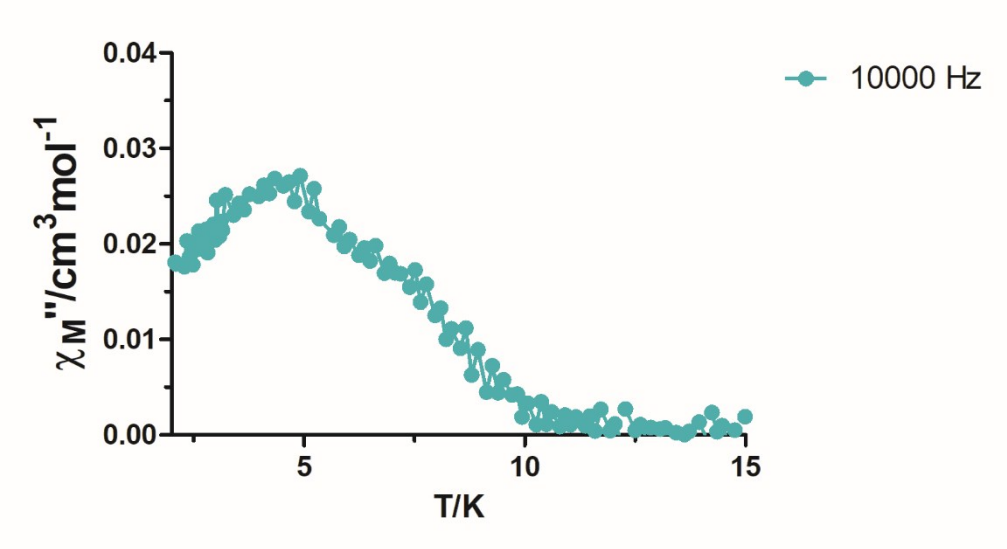

Figure S31. Temperature dependence of out-of-phase component of the *ac* susceptibility in a *dc* applied field of 1000 Oe for the diluted sample (Y/Dy = 10/1) of compound **3**.

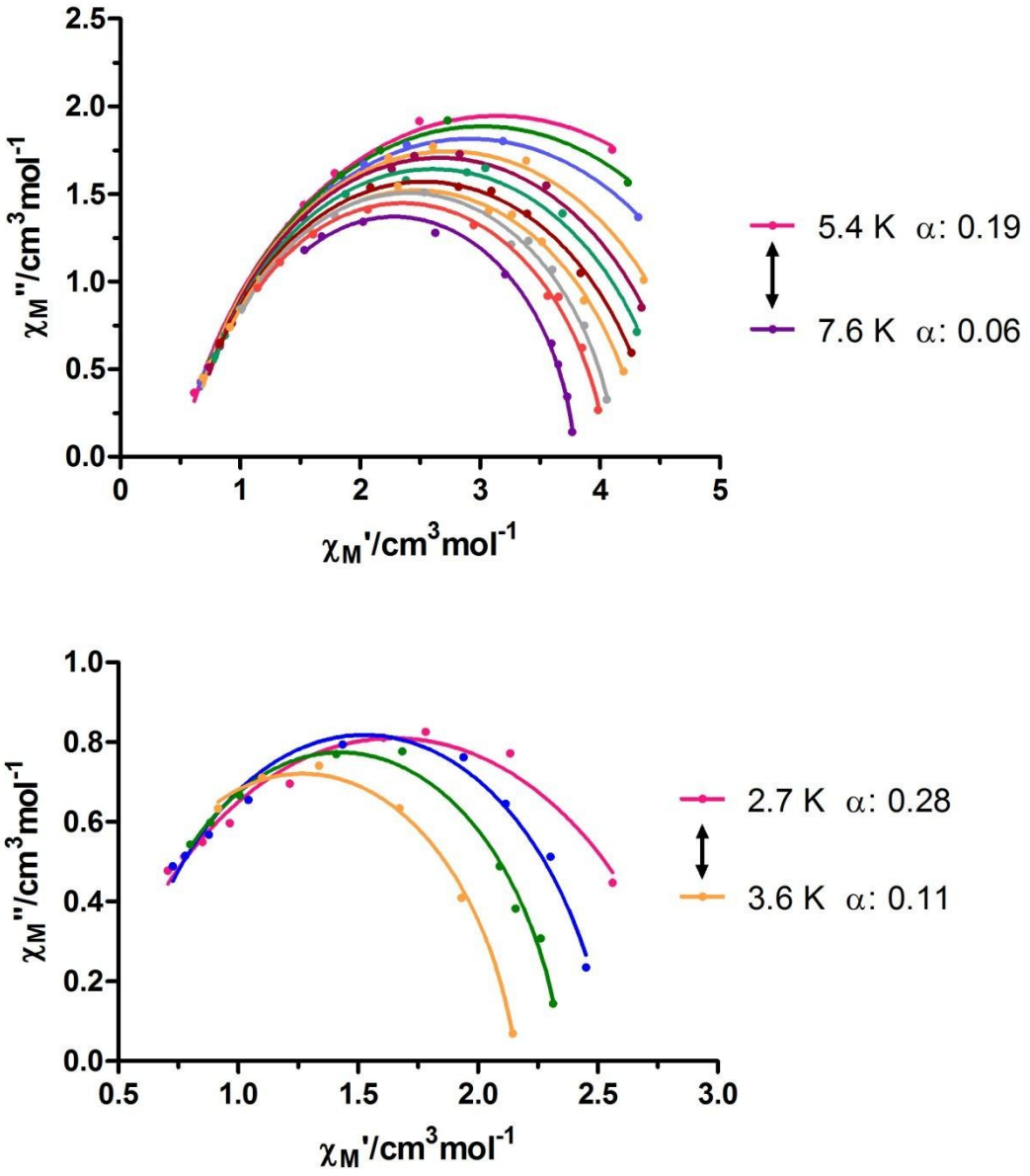

Figure S32. Cole-Cole plots in a *dc* applied field of 1000 Oe for **1** (up) and **2** (bottom).

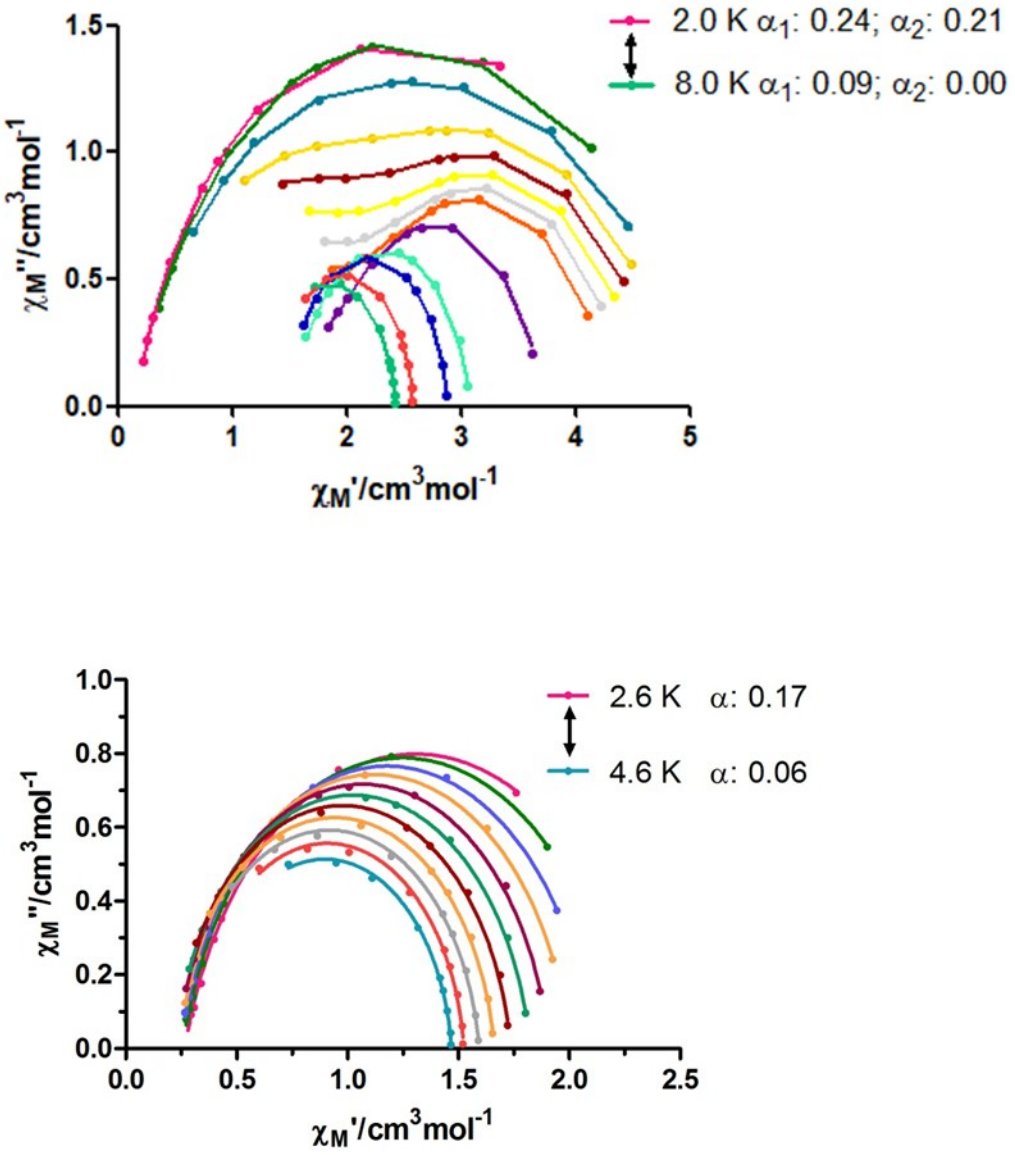

Figure S33. Cole-Cole plots in a *dc* applied field of 1000 Oe for **3** (up) and **4** (bottom).

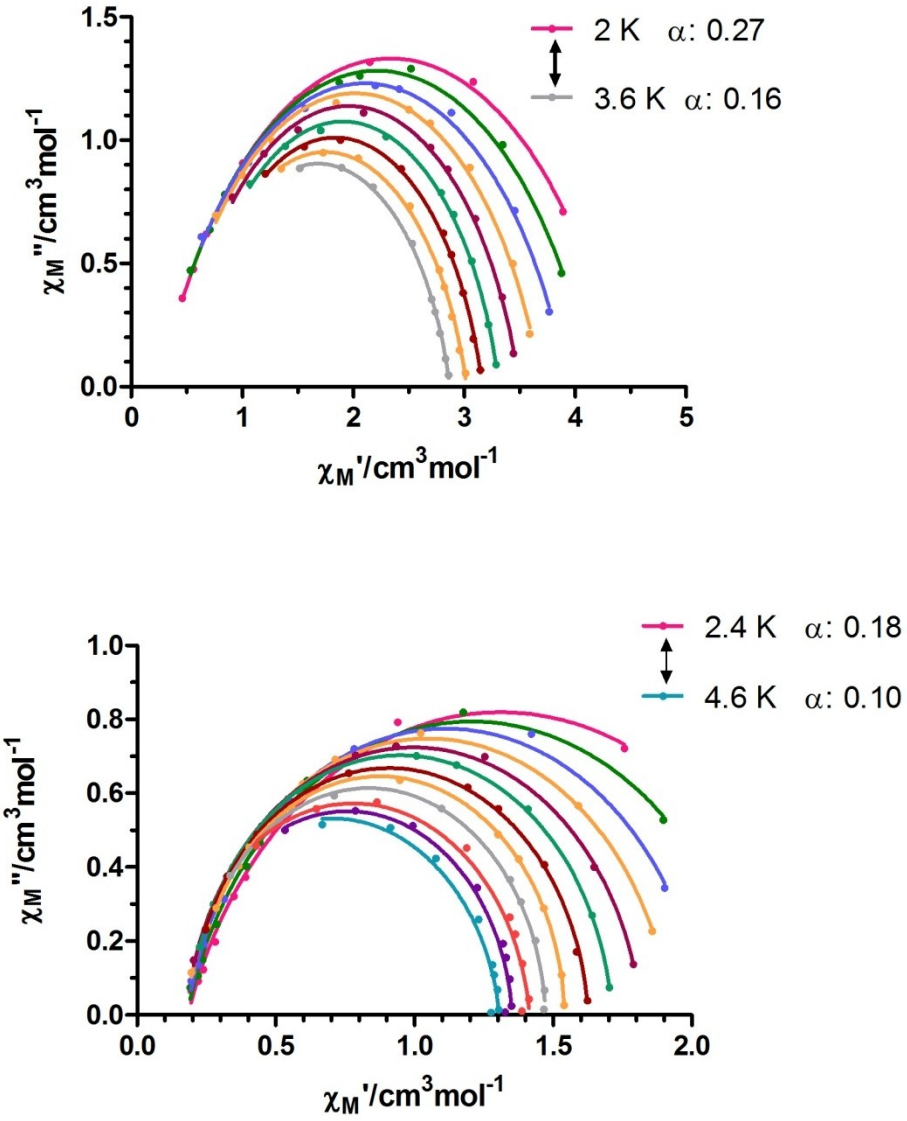

Figure S34. Cole-Cole plots in a *dc* applied field of 1000 Oe for **5** (up) and **6** (bottom).

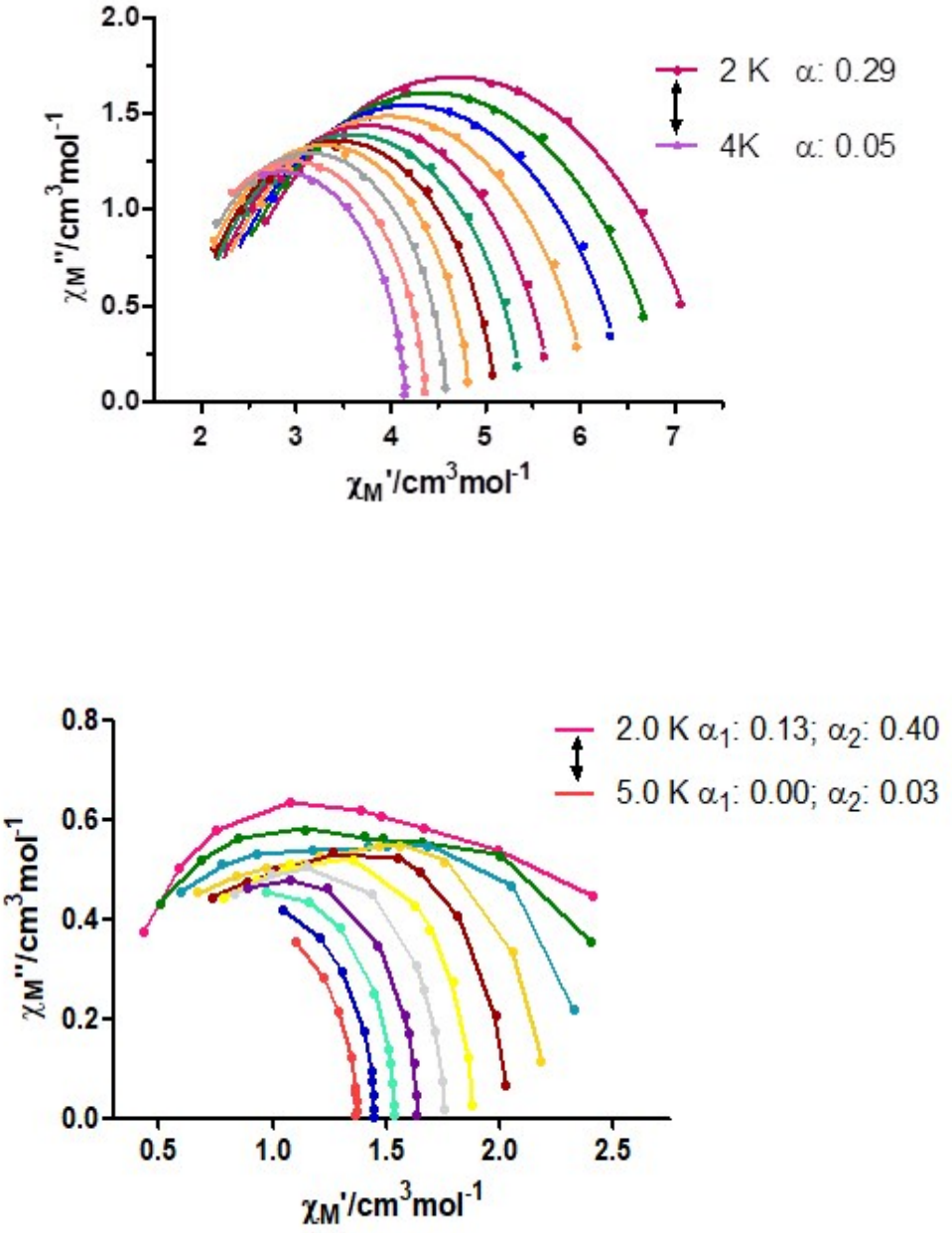

Figure S35. Cole-Cole plots in a *dc* applied field of 1000 Oe for **8** (up) and **10** (bottom).

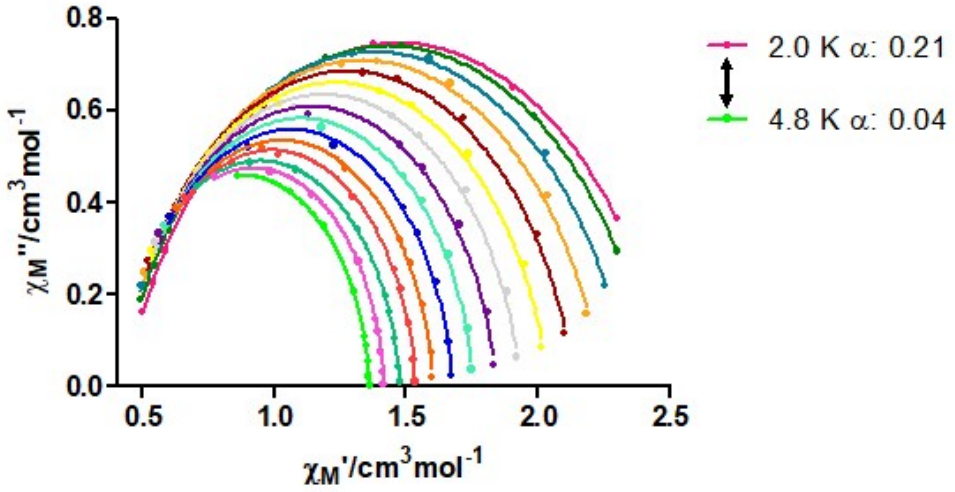

Figure S36. Cole-Cole plots in a *dc* applied field of 1000 Oe for **11**.

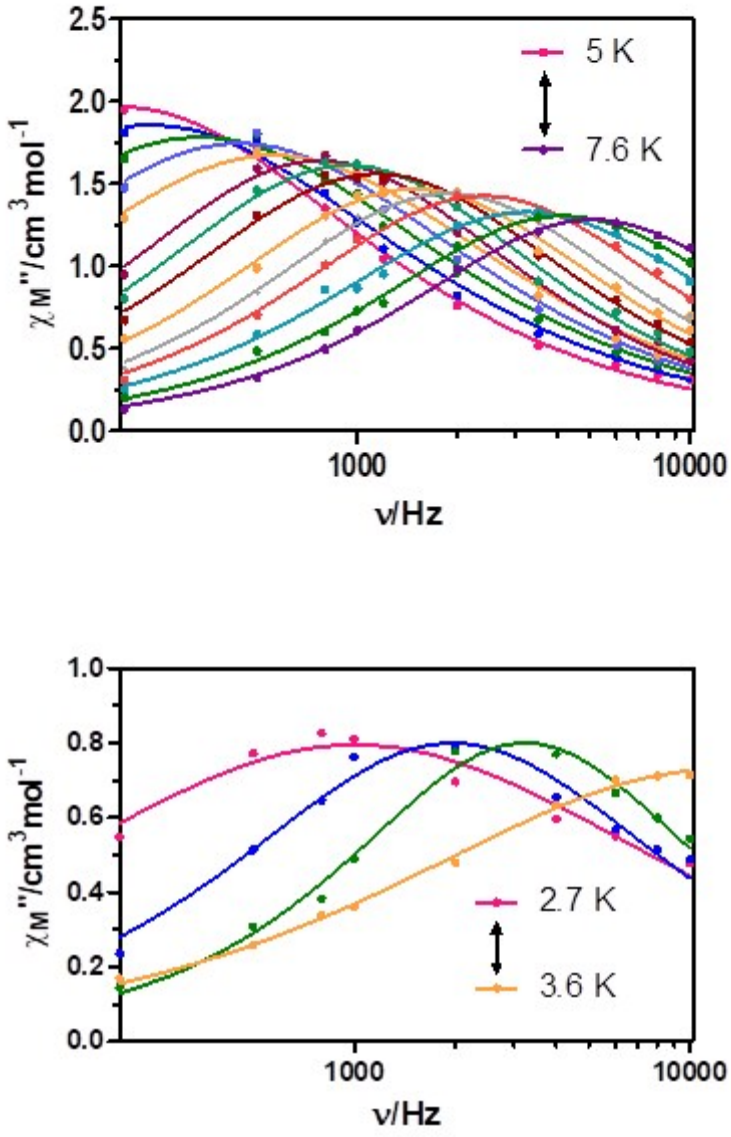

Figure S37. Variable-temperature frequency dependence of the χ_M'' signal under 1000 Oe applied field for **1** (up) and **2** (bottom). Solid lines represent the best fitting of the experimental data to the Debye model.

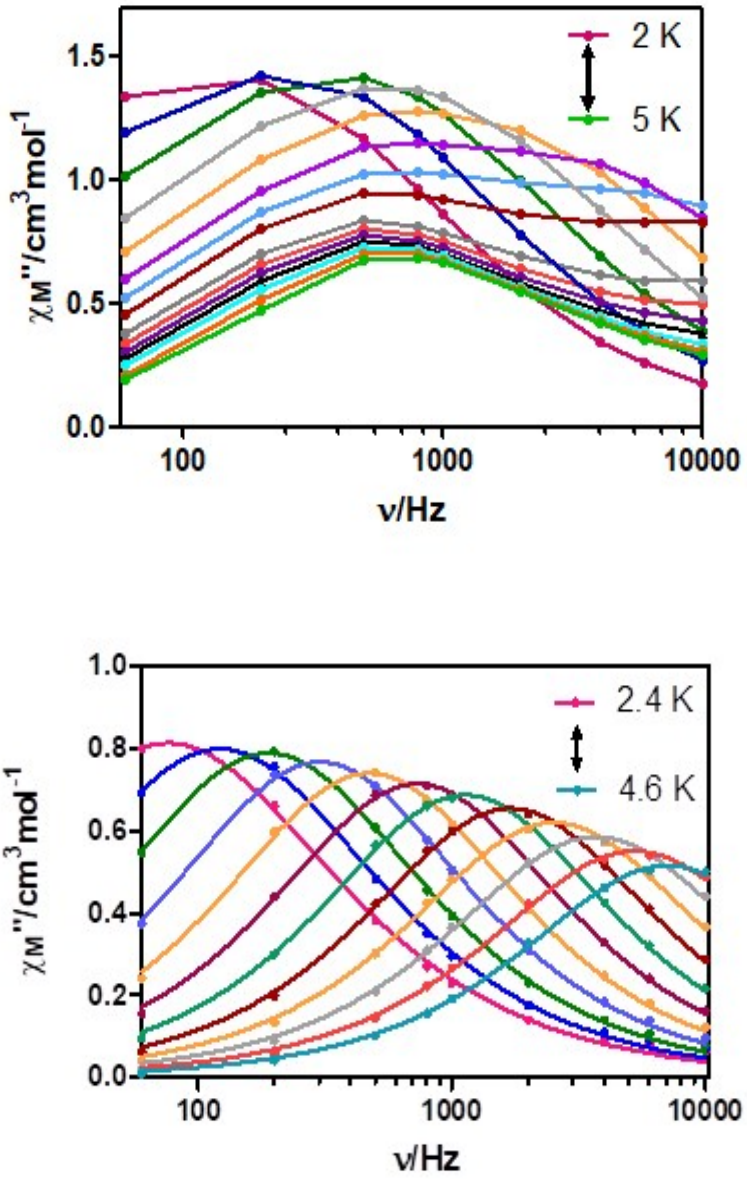

Figure S38. Variable-temperature frequency dependence of the χ_M'' signal under 1000 Oe applied field for **3** (up), **4** (bottom). Solid lines represent the best fitting of the experimental data to the Debye model for compound **4.**

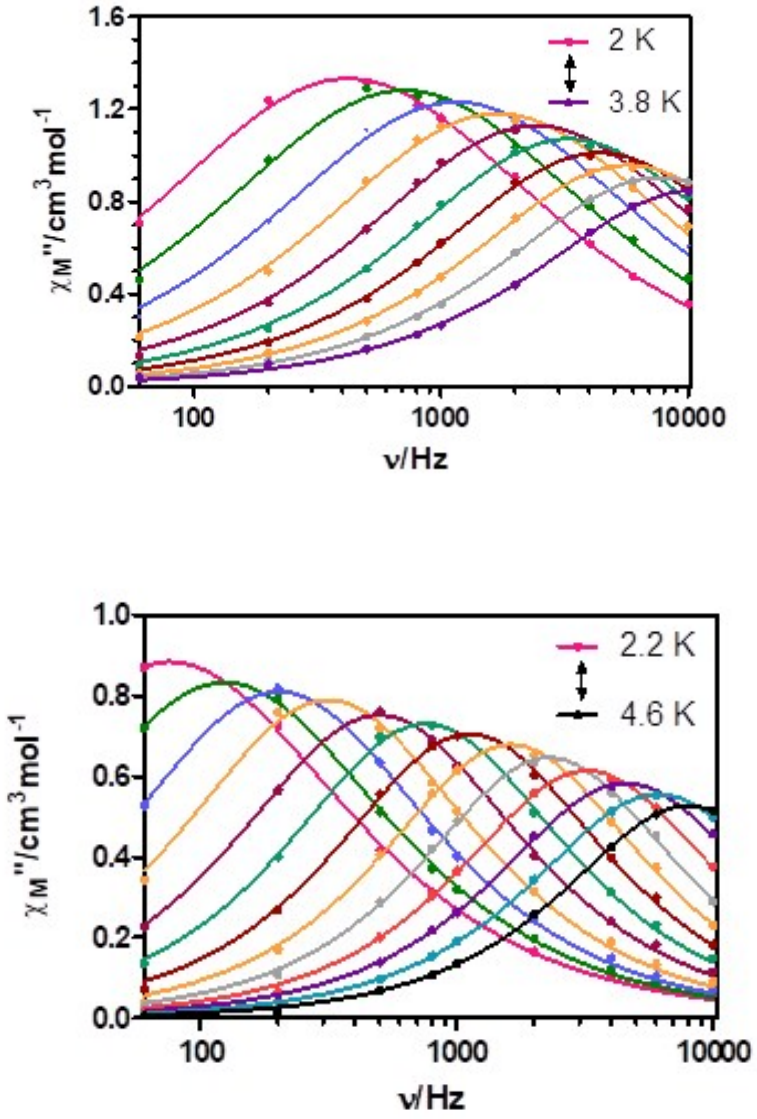

Figure S39. Variable-temperature frequency dependence of the χ_M'' signal under 1000 Oe applied field for **5** (up), **6** (bottom). Solid lines represent the best fitting of the experimental data to the Debye model for compounds **5** and **6.**

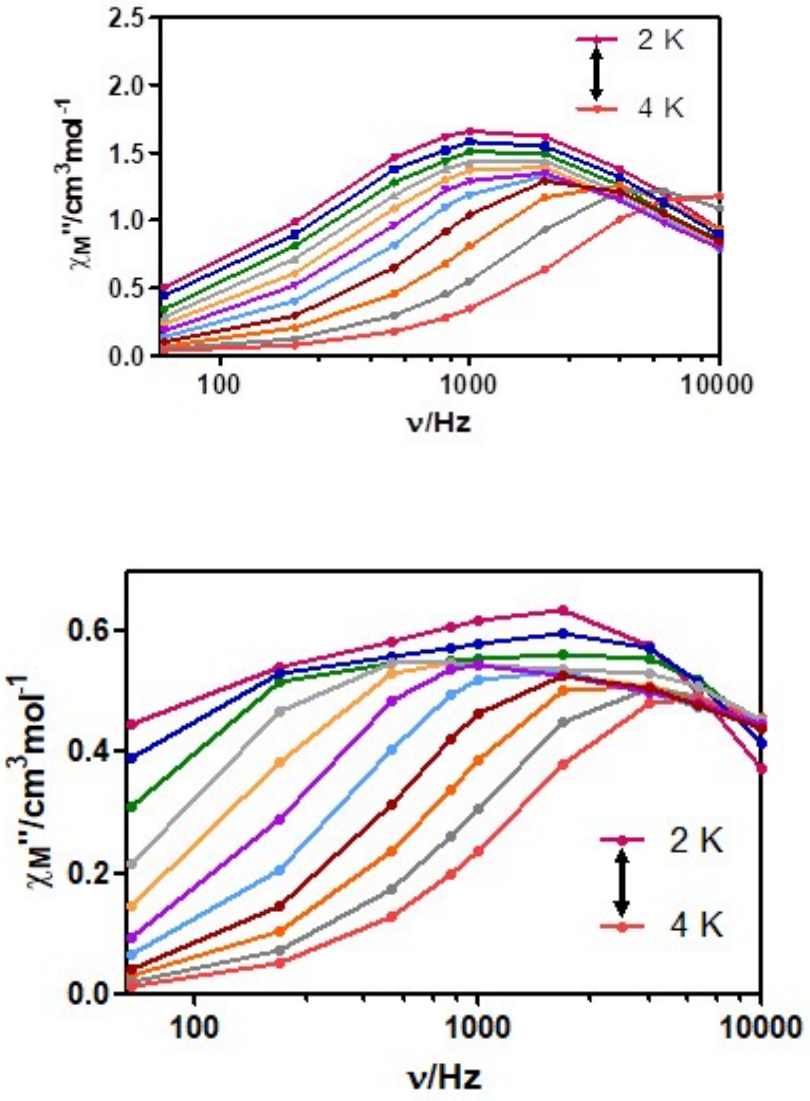

Figure S40. Variable-temperature frequency dependence of the χ_M'' signal under 1000 Oe applied field for **8** (up) and **10** (bottom). Solid lines represent the best fitting of the experimental data to the Debye model for compound **8**.

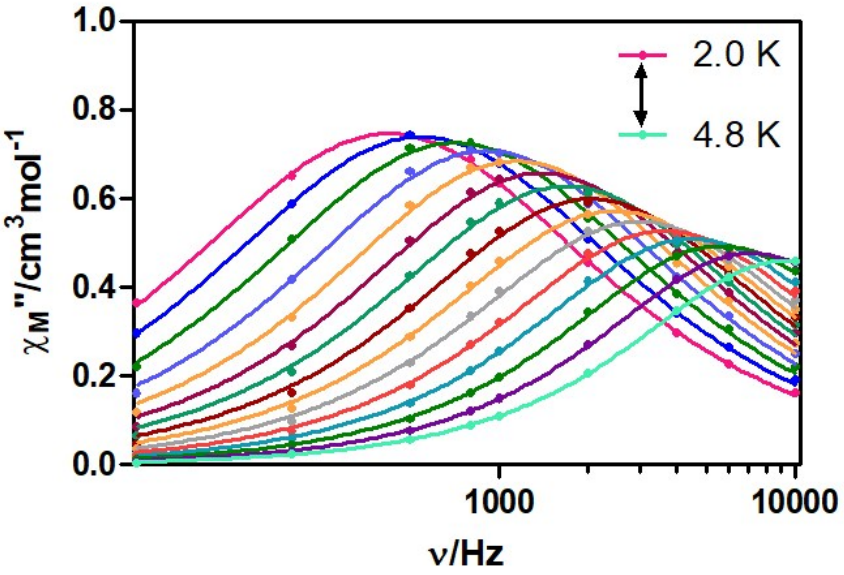

Figure S41. Variable-temperature frequency dependence of the χ_M" signal under 1000 Oe applied field for **11.** Solid lines represent the best fitting of the experimental data to the Debye for compound **11**.

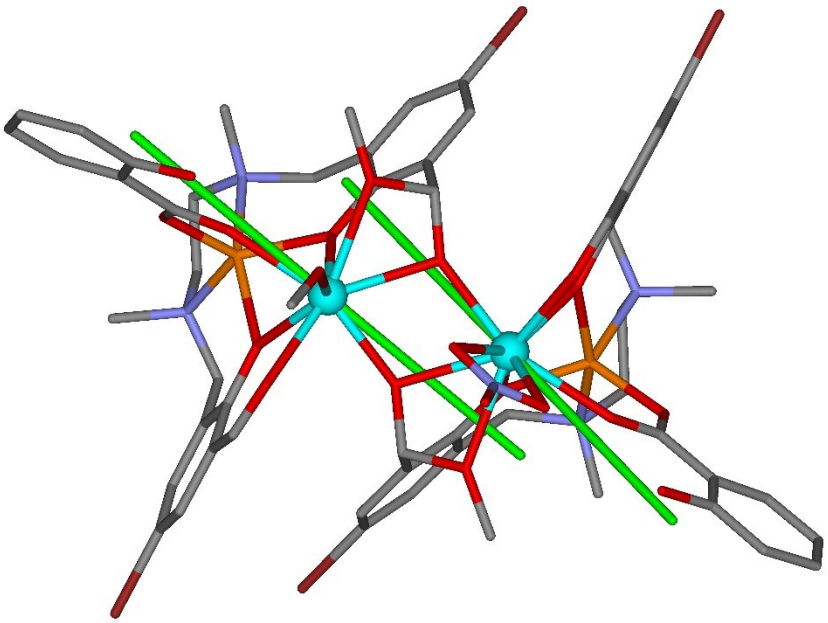

Figure S42. Theoretical orientation of the magnetic moments (green lines) for Dy(III) ions in compound **7**.

Table S6. Relaxation Fitting Parameters from Least-Squares Fitting of χ(φ) data for complex **3**.

T (K)	FR		SR	
	α_1	τ_1	α_2	τ_2
2.4	0.2510	2.75E-04	-	-
2.8	0.2002	5.79E-05	-	-
3.1	0.1705	2.01E-05	0.3066	3.58E-04
3.3	0.2348	1.21E-05	0.2744	3.69E-04
3.5	0.3405	6.62E-06	0.2400	3.74E-04
3.7	0.3963	3.96E-06	0.2240	3.63E-04
3.9	0.4707	2.40E-06	0.2084	3.52E-04
4.2	0.5655	1.14E-06	0.1812	3.26E-04
4.8	0.5820	2.78E-07	0.1574	2.58E-04
5.4	-	-	0.1430	1.89E-04
6.0	-	-	0.1202	1.28E-04
6.6	-	-	0.0988	8.21E-05
7.5	-	-	0.0905	3.83E-05
8.0	-	-	0.0901	2.44E-05

Table S7. Relaxation Fitting Parameters from Least-Squares Fitting of χ(φ) data for complex **10**.

T (K)	FR		SR	
	α_1	τ_1	α_2	τ_2
2.3	0.2419	4.41E-05	0.1901	8.82E-04
2.6	0.3119	3.40E-05	0.0734	5.32E-04
2.9	0.2978	2.37E-05	0.0358	2.87E-04
3.2	0.2513	1.65E-05	0.0372	1.60E-04
3.5	0.1657	1.24E-05	0.0309	9.52E-05
3.8	0.0972	9.38E-06	0.0356	5.89E-05
4.1	0.0000	7.80E-06	0.0440	3.81E-05
4.4	0.0000	6.18E-06	0.0276	2.83E-05
4.7	0.0000	6.47E-06	0.0175	2.34E-05

8. Luminescence properties.

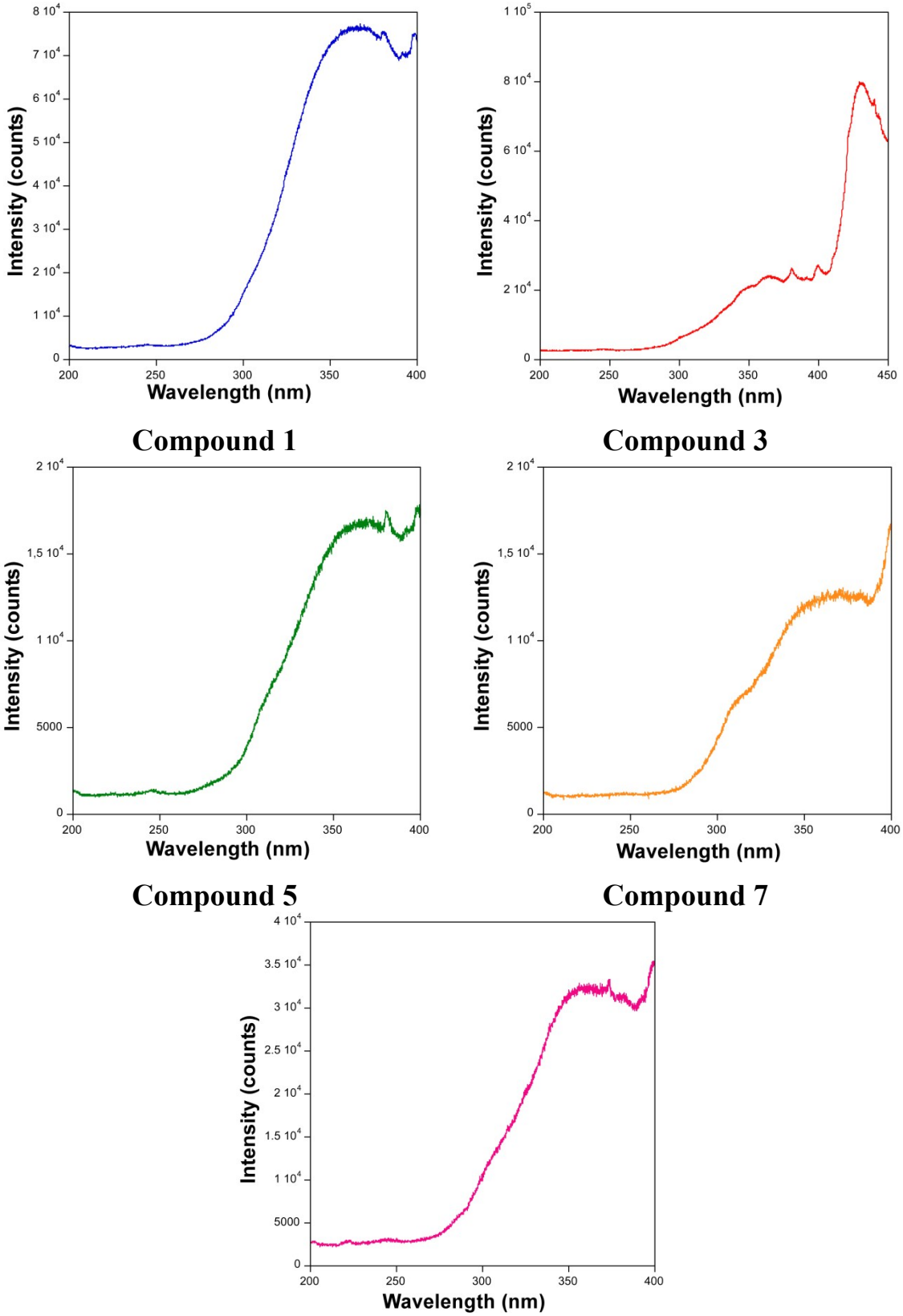

Figure S43. Excitation spectra of all Dy-based compounds.

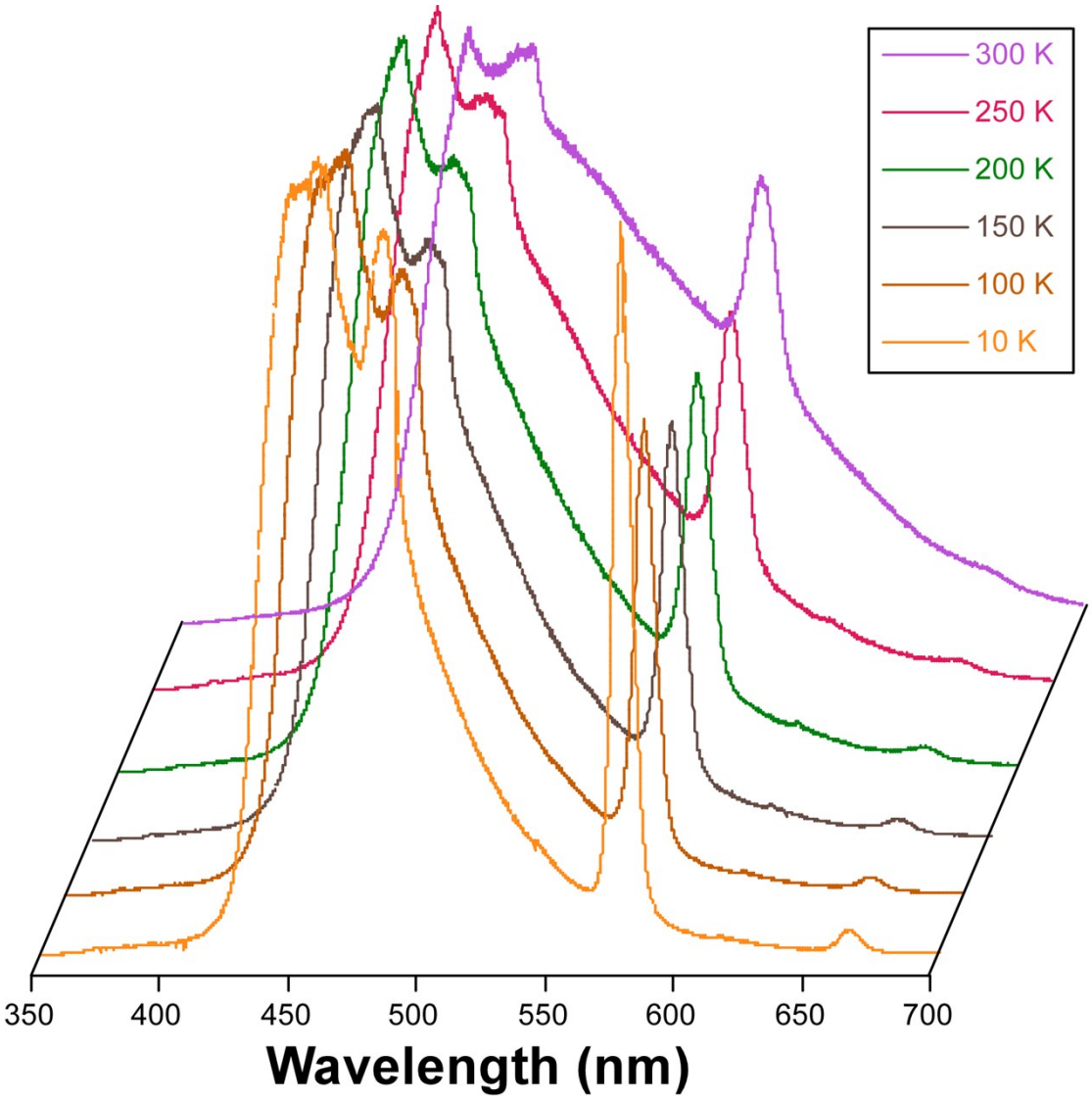

Figure S44. Temperature-dependent emission of compound **7**.

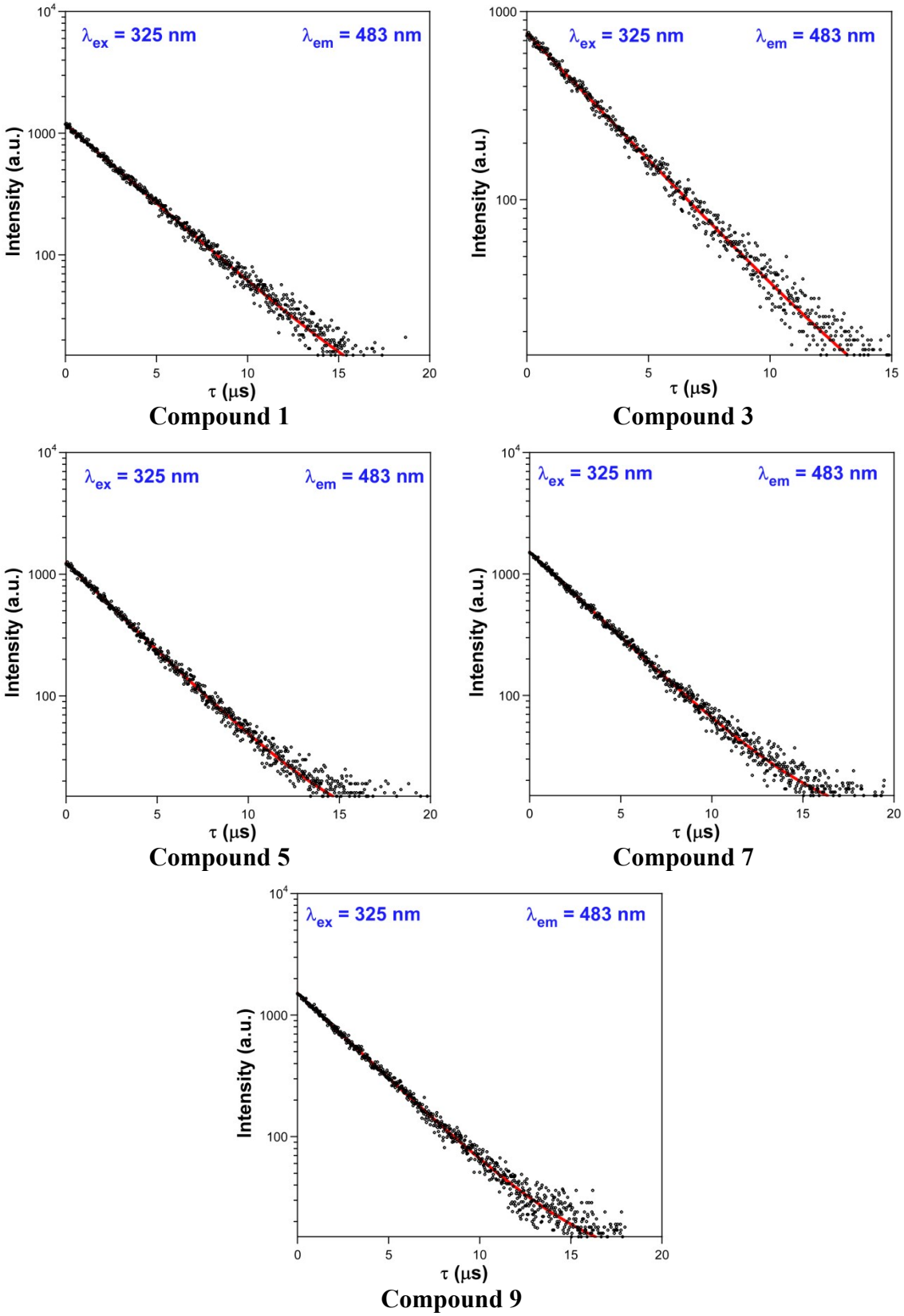

Figure S45. Luminescence decay lifetime fits at $^4F_{9/2} \rightarrow {}^6H_{15/2}$ transition for Dy-based compounds.

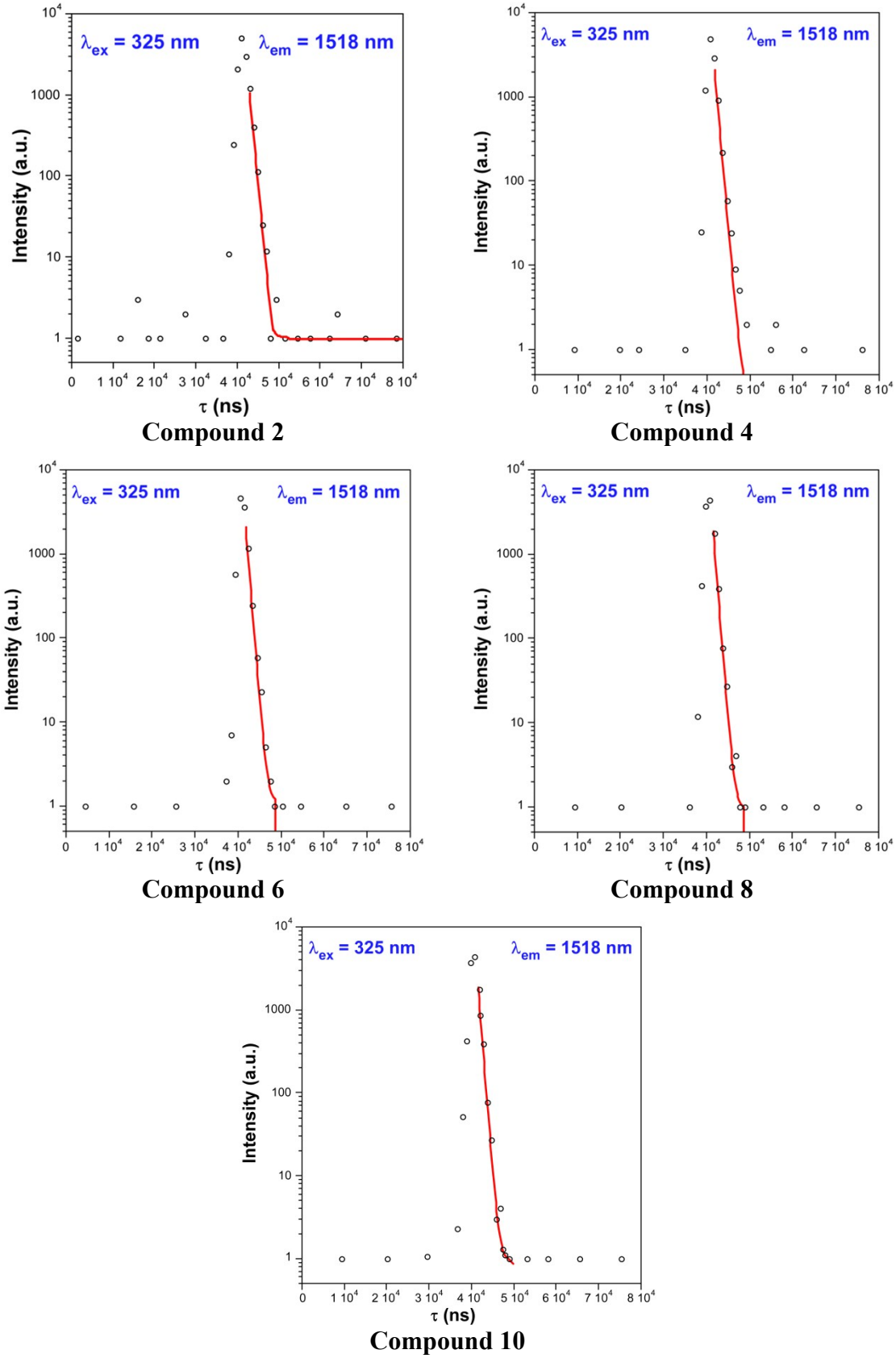

Figure S46. Luminescence decay lifetime fits monitored at $^4I_{13/2} \rightarrow {}^4I_{15/2}$ transition for Er-based compounds.